

# Numerical comparison of drug concentrations in different drug eluting stent designs using 2D models

---

**Meštrović, Nikolina**

**Master's thesis / Diplomski rad**

**2025**

*Degree Grantor / Ustanova koja je dodijelila akademski / stručni stupanj:* **University of Zagreb, Faculty of Science / Sveučilište u Zagrebu, Prirodoslovno-matematički fakultet**

*Permanent link / Trajna poveznica:* <https://um.nsk.hr/um:nbn:hr:217:060557>

*Rights / Prava:* [In copyright](#)/[Zaštićeno autorskim pravom.](#)

*Download date / Datum preuzimanja:* **2025-03-29**



*Repository / Repozitorij:*

[Repository of the Faculty of Science - University of Zagreb](#)



**UNIVERSITY OF ZAGREB  
FACULTY OF SCIENCE  
DEPARTMENT OF MATHEMATICS**

Meštrović, Nikolina

**NUMERICAL COMPARISON OF DRUG  
CONCENTRATIONS IN DIFFERENT  
DRUG ELUTING STENT DESIGNS  
USING 2D MODELS**

Diploma thesis

Zagreb, February, 2025.

Ovaj diplomski rad obranjen je dana \_\_\_\_\_ pred ispitnim povjerenstvom u sastavu:

1. \_\_\_\_\_, predsjednik
2. \_\_\_\_\_, član
3. \_\_\_\_\_, član

Povjerenstvo je rad ocijenilo ocjenom \_\_\_\_\_.

Potpisi članova povjerenstva:

1. \_\_\_\_\_
2. \_\_\_\_\_
3. \_\_\_\_\_

# Table of contents

<b>Table of contents</b>	<b>iii</b>
<b>Introduction</b>	<b>2</b>
<b>1 Coronary artery disease</b>	<b>3</b>
1.1 Cardiovascular system . . . . .	3
1.2 Atherosclerosis . . . . .	5
1.3 Coronary artery disease and PCI . . . . .	10
1.4 PCI and stent implantation . . . . .	14
1.5 Pharmacological component of PCI and DES . . . . .	14
<b>2 Drug eluting stents</b>	<b>17</b>
2.1 Stent platform and geometry . . . . .	17
2.2 Stent coating . . . . .	18
<b>3 Model of controlled drug release</b>	<b>21</b>
3.1 3D model of controlled drug release . . . . .	21
3.2 Polymer coating - 1D domain . . . . .	26
3.3 Higuchi's equation - perfect sink conditions . . . . .	27
3.4 In vivo model . . . . .	31
3.5 2D model for controlled drug release . . . . .	34
<b>4 Numerical simulations</b>	<b>41</b>
4.1 Approximating parameters of the model . . . . .	41
4.2 Results of numerical simulations . . . . .	45
<b>Bibliography</b>	<b>59</b>

# Introduction

Coronary artery disease (CAD), sometimes also called ischemic heart disease or coronary heart disease, is a pathological condition characterized by narrowed or obstructed coronary arteries. Presentations of the disease are various and depend on the location and severity of the narrowing or obstruction. Coronary arteries supply oxygen rich blood to the heart muscle, and disturbance of the blood flow in such arteries can lead to myocardial ischemia or infarction. Atherosclerosis is the most common underlying condition that leads to narrowing or blockage of coronary arteries.

Mechanical revascularization aims to remove the obstruction and can generally be performed in two different ways, by coronary artery bypass grafting (CABG) or percutaneous coronary intervention (PCI). Our interest lies in PCI that is accompanied by implantation of drug eluting stent, a tubular wire-mesh device coated with drug eluting layer.

We will first give a brief overview of cardiovascular system in order to set the baseline understanding of function of arteries as its component. Secondly, we delve in current understanding of pathophysiology of atherosclerosis. Next we take a look at CAD manifestations in clinical practice, classified as chronic or acute coronary syndromes with focus on CAD presentation in which PCI is recommended and we briefly describe PCI procedure with stent implantation. Such information is acquired in order to get basic understanding of CAD, mechanisms of development of atherosclerosis and some technical aspects of stent delivery that help us understand how drug eluting stent should work to be effective and ways in which it can fail.

In order to model this problem mathematically, we propose a coupled diffusion/dissolution model in the stent coating and transport of drug into artery model in the artery. To derive the mathematical model we consider multiple models with focus on diffusion/dissolution models. In order to apply the model for specific combination of drug and polymer coating it is imbedded in, in our case sirolimus in non-degradable polymer matrix, we need to estimate parameters of the model.

Estimating parameters proved to be a hard task due to lack of available information in the literature. Part of the parameters, parameters associated with transport of drug in the artery model, is taken from in vivo studies. Parameters associated with diffusion/dissolution model are estimated from data available in in vitro studies by utilizing Higuchi's equation.

We aim to compare effectiveness of different stent geometries with identical polymer matrix and therapeutic agent. We conduct numerical simulations on 3 different stent cell geometries and compare the results.

# Chapter 1

## Coronary artery disease

### 1.1 Cardiovascular system

Arteries are part of the cardiovascular system, a complex transport system that has a crucial role in maintaining homeostasis. The heart acts as a pump that moves blood through the elaborate system of blood vessels. Blood is a viscous fluid composed of plasma and blood cells. Plasma is the liquid component, a solution of electrolytes, proteins, lipids, carbohydrates and waste products. Cardiovascular system regulates composition of interstitial fluid by continuously exposing it to circulating plasma. Substances present in plasma are transported between organs by convection via blood vessels. Smallest blood vessels, capillaries, cast a wide network and permeate all tissues in the body. Distance from any cell to the nearest capillary is never more than approximately  $10^{-6}$  m and solutes are exchanged between plasma and interstitial fluid efficiently by diffusion. [1]

Functionally, there are two circulatory pathways, pulmonary and systemic. In pulmonary circulation deoxygenated blood is transported from the right ventricle to the lungs, oxygenated in the lungs and transported back to the left atrium. In systemic circulation oxygenated blood is transported from the left ventricle to the body and deoxygenated blood is returned to the right atrium. Left ventricle pumps around 3% of cardiac output into coronary arteries to supply heart muscle with oxygenated blood, see [1].

On the path from left ventricle blood passes through the aorta, the largest artery and carries on to arteries, arterioles, capillaries, venules and veins to finally enter the right atrium via vena cava, the largest vein. These continuous vascular sections differ in size, function and morphological characteristics.

All blood vessels feature endothelium, monolayer of endothelial cells that is in direct

contact with blood. Arteries have a thick wall that contains smooth muscle, elastin and collagen fibers. Large proportion of elastin fibers allows arteries to stretch under pressure to conduct blood pumping out of the heart. Resistance to flow is relatively low and stable. Luminal diameter of aorta is approximately 25 mm and smallest arteries have luminal diameter of approximately 0.1 mm. In comparison to arteries, arterioles have smaller luminal diameter, thicker wall relative to luminal diameter, larger proportion of smooth muscle cells and smaller proportion of elastin fibers. Resistance to flow is high and variable, allowing for regulation of blood flow through particular organs. Capillaries have smallest luminal diameter of approximately 0.005 mm and consist only of endothelium. Endothelium is approximately 0.001 mm thick, separates blood from interstitial fluid and allows for diffusion across the wall. Venous vessels collect blood leaving the capillaries. Their thin walls contain smooth muscle cells and expand or restrict passively in response to changes in pressure across the vessel wall. Presence of one way valves in veins and venules prevents reverse blood flow. See [1].

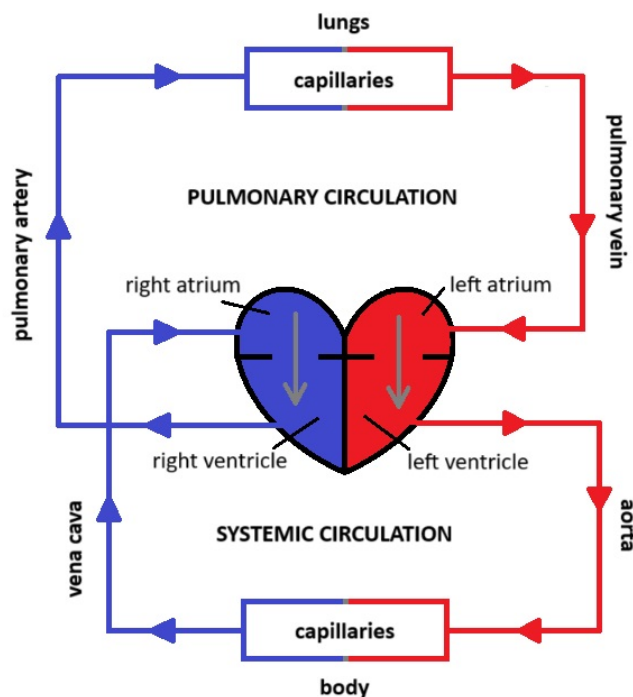


Figure 1.1: Simplified scheme of pulmonary and systemic circulation.

In the following subsections we will give a summary of our current understanding of atherosclerosis, its implications in CAD and current guidelines for treatment of CAD.

## **1.2 Atherosclerosis**

Atherosclerosis is a widespread, progressive disease that predominantly affects large and medium-sized arteries. The main feature of atherosclerosis is accumulation of lipids, fibrous elements, and calcification in the artery wall, see [1], [2].

Atherosclerosis used to be viewed as segmental or localized disease characterized by stenosis, abnormal narrowing of artery visible by angiography. It was considered primarily a cholesterol storage disease. Treatment was focused on mechanical revascularization of affected sites. Later findings challenged such understanding as emerging evidence pointed to crucial role of inflammation in pathophysiology of atherosclerosis. We currently view atherosclerosis as an inflammatory disorder, see [3]. Approach to treatment of atherosclerosis, and by extension CAD, has undergone significant changes. Before we get to latest approaches and guidelines for treatment of CAD we will look at current understanding of pathophysiology of atherosclerosis.

Next we give overview of mechanisms that underlie development of atherosclerosis, based on review article written by Shifa Jebari-Benslaiman, Unai Galicia-García and others, see[2].

### **Pathophysiology of atherosclerosis**

Atherosclerotic plaque formation is initiated by endothelial dysfunction that leads to fatty streak formation. In later stages we observe formation of fibrous plaque that can potentially rupture.

Endothelium faces luminal side of all arteries. It is in direct contact with circulating blood. Endothelium is sensitive to changes in circulating blood and mechanical forces acting on the arterial wall. It transmits perceived signals to the blood, tunica media and adventitia by production of biologically active substances. It can produce coagulants, anti-coagulants, vasodilators, vasoconstrictors, pro-inflammatory and anti-inflammatory molecules. Endothelium acts as a mediator for homeostasis, inflammatory and immune response and cellular proliferation in the arterial wall. Endothelium also maintains non-adhesive luminal surface.

Endothelial dysfunction leads to disturbance in mechanisms involved in maintenance of vascular homeostasis. Artery segments in which endothelial dysfunction occurs are prone

to vasoconstriction, lipid infiltration, leukocyte adhesion, platelet activation and oxidative stress which provoke inflammatory response.

High concentration of low-density lipoprotein in circulating plasma heightens the incidence of transendothelial infiltration of LDLs to the subendothelium. LDLs cross the endothelium by diffusion, paracellularly (passing through the intercellular space) or by transcytosis (transport of material through the cell in a membrane coated vesicle). In the subendothelium LDLs undergo modifications, most commonly oxidative. Modified LDLs act as an inflammatory agent that promotes atherosclerotic formation.

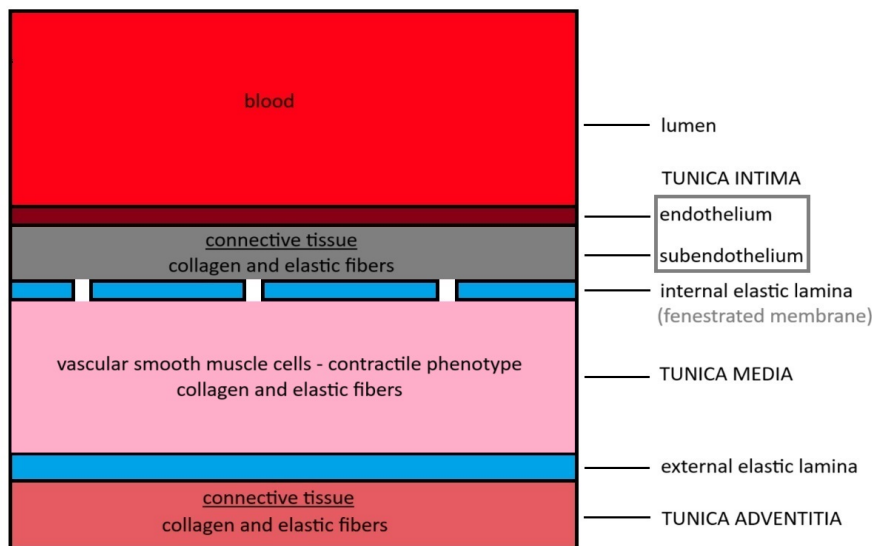


Figure 1.2: Scheme of cross-section of healthy artery wall.

In response to inflammatory agents endothelium can undergo short term phenotypic modulation (endothelial type I activation) or sustained phenotypic modulation (endothelium type II activation). Endothelium type II activation is provoked only by certain pro-inflammatory agents. Modified LDLs contribute to such activation of endothelial cells (ECs). This type of activation of ECs leads to complex inflammatory response resulting in secretion of chemokines and pro-thrombotic mediators, and upregulated expression of leukocyte adhesion molecules.

Activated ECs start the process of monocyte recruitment into subendothelium. Monocytes roll over activated endothelium area and become activated by endothelial surface

bound chemokines. At some point rolling stops and monocyte binds to the endothelium due to increased expression of adhesion molecules of activated ECs. Next, transmigration of activated monocytes into subendothelium, led by chemokines, occurs.

In subendothelium, activated monocytes differentiate into macrophages. Macrophages can be polarized into M1 phenotype (pro-inflammatory) or M2 phenotype (anti-inflammatory), depending on inflammatory environment, due to macrophage plasticity. M1 phenotype predominates in disease progression and M2 in regression. M1 phenotype promotes monocyte recruitment and inflammatory response propagation. Macrophages also express multiplicity of receptors that mediate the internalization of modified and non-modified LDLs. Expression of some of the receptors that mediate internalization of modified LDLs is not downregulated by cholesterol uptake. In presence of high content of modified LDLs, macrophages internalize larger amounts of modified LDLs. Pro-inflammatory microenvironment hinders efflux system for removal of excess cholesterol in macrophages. Lipid-laden macrophages, also called foam cells, accumulate, and induce growth of atherosclerotic lesion. Foam cells further aggravate inflammatory response.

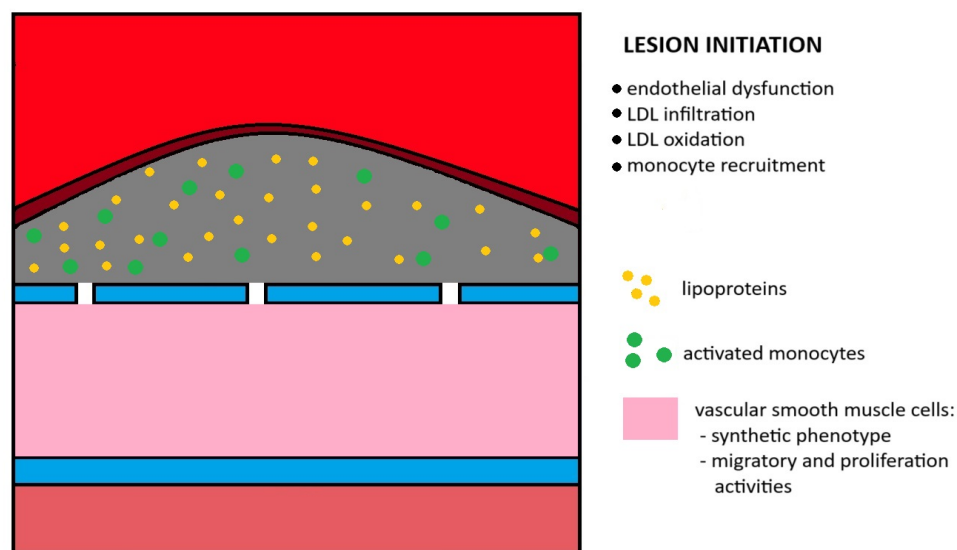


Figure 1.3: Scheme of cross-section of artery wall in initial stage of atherosclerosis.

Vascular smooth muscle cells (VSMCs) have contractile phenotype in healthy artery. Their main function is regulation of blood vessel diameter and blood flow. In atherosclerotic segment of the artery VSMCs have synthetic phenotype that allows for migratory

and proliferation activity. VSMCs migrate to subendothelium. Once in subendothelium VSMCs are also able to internalize modified LDL and do so in an unregulated fashion. Lipid-laden VSMCs constitute at least 50% of foam cell population in subendothelium. Accumulation of cholesterol in subendothelium also promotes formation of cholesterol crystals inside and outside of cells. Accumulation of foam cells, cholesterol crystals and LDL forms a fatty streak.

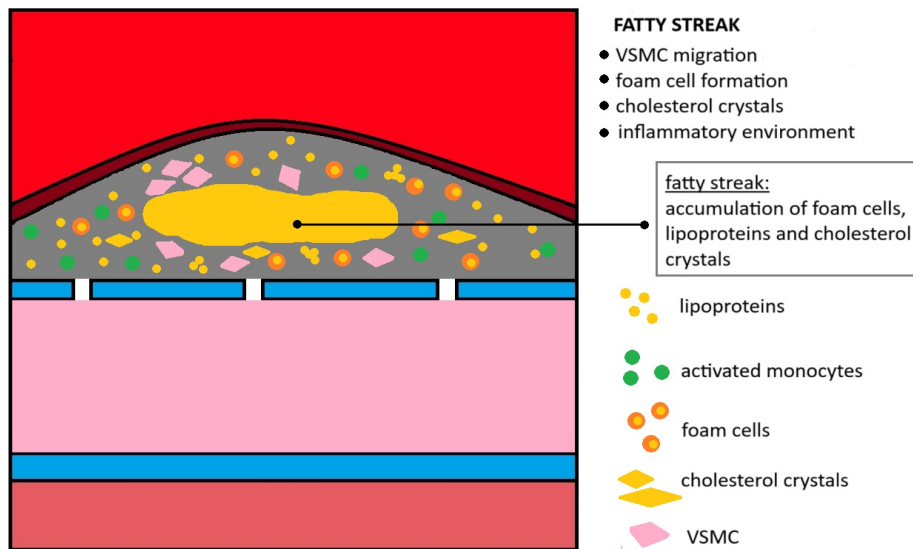


Figure 1.4: Scheme of cross-section of artery wall, fatty streak formation. VSMC; vascular smooth muscle cells.

Fatty streak increases in size because of persistent loop of LDL infiltration, monocyte recruitment and foam cell formation. Eventually, it develops necrotic core, a cell free, lipid rich area and fibrous cap, subendothelial barrier between lumen and necrotic core. Development of necrotic core and fibrous cap marks transition of fatty streak into fibrous plaque.

VSMCs that have migrated to the luminal side of the artery, along with extracellular matrix (ECM) derived from VSMCs, form a fibrous cap. VSMC proliferate in the intima due to production of growth factors by foam cells and ECs. VSMCs have the synthetic phenotype that allows for increased production of ECM components, collagen, elastin and proteoglycans.

Necrotic core is located at the nucleus of atherosclerotic plaque. It is a cell free, lipid rich area with reduced supporting collagen. Apoptosis enhances in the macrophage and VSMCs population due to increased oxidative stress, activation of receptors involved in death signaling, inhibition of survival pathways, and nutrient deprivation. Necrotic core increases in size due to cell death combined with impaired efferocytosis, a process that removes apoptotic cells. Instead, secondary necrosis occurs, an autolytic process of cell disintegration with release of cell components. Released components include oxidative and inflammatory components, lipids and cholesterol crystals. Release of these components accelerates death of neighboring cells and furthers accumulation of lipids and cholesterol crystals in subendothelial space.

Among released components there are also matrix metalloproteinases (MMP) and tissue factor. MMPs are able to degrade ECM proteins and reduce size of fibrous cap, and tissue factor increases thrombogenicity of necrotic core. Fibrous cap gives structural support that prevents rupture of atherosclerotic plaque. In case of rupture subendothelial space and necrotic core are exposed to circulating blood, triggering thrombosis.

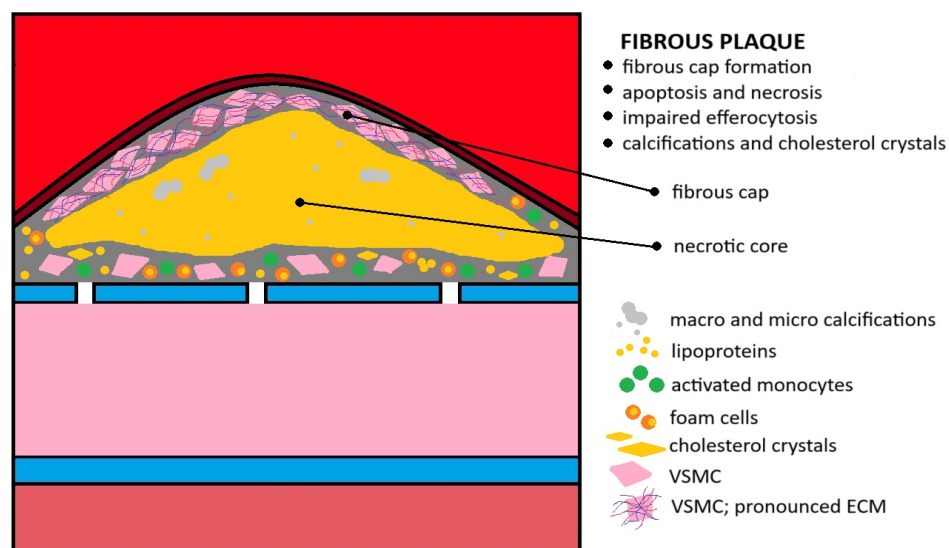


Figure 1.5: Scheme of cross-section of artery wall with fibrous plaque. VSMC; vascular smooth muscle cells. ECM; extracellular matrix.

Calcification can occur in necrotic core of advanced atherosclerotic plaques. M1 macrophages promote the initial microcalcification formation. Microcalcification can occur as a

consequence of apoptosis of macrophages and VSMCs or VSMC differentiation into early phase osteoblasts. M2 macrophages can promote macroscopic calcium deposition by induction of osteoblastic differentiation and maturation of VSMCs. Macrocalcification is positively correlated with plaque stability and microcalcifications are positively correlated with plaque rupture, see [4].

### **Vulnerable plaque, plaque rupture and thrombus formation**

Fibrous plaque is considered vulnerable if it has high probability of rupture. Characteristic of such plaque include large necrotic core, thin fibrous cap and increased inflammatory response. Increased inflammation plays a crucial role in fibrous plaque rupture because it promotes instability of the fibrous cap. Increased localized inflammation, in the cap and shoulders of the plaque, causes death of VSMCs, and matrix metalloproteinases present in necrotic core degrade ECM, the building blocks of fibrous cap. Thin cap is prone to rupture when exposed to hemodynamic forces.

Once the plaque ruptures subendothelial space is exposed to circulating blood and coagulation process is initiated to cover the wound. Platelets adhere to the subendothelial collagen and become activated. This induces recruitment and aggregation of more platelets in an effort to heal the wound. Released prothrombotic elements from necrotic core in contact with plasma result in thrombin production. Thrombin converts fibrinogen to fibrin threads that cover the lesion by forming stable and well arranged structure called thrombus.

This process is initiated with the goal of wound healing but complications often occur. One of the complications is detachment of thrombus from the artery wall that produces a clot i.e. embolus. Embolus circulates in the cardiovascular system and eventually gets stuck in distal blood vessel causing blood flow obstruction. Another complication occurs because thrombus triggers range of reactions to make the lesion more stable and less prone to rupture. This causes thickening of the plaque and risk of vessel obstruction increases.

## **1.3 Coronary artery disease and PCI**

As mentioned before, manifestations of CAD are varied. Manifestations of CAD that are of interest to us are ones that require revascularization, specifically revascularization by PCI, percutaneous coronary intervention. PCI is minimally invasive procedure used to open occluded blood vessel. Common part of PCI is implantation of stent in the previously occluded blood vessel. Procedure is described in more detail in section 1.4. PCI is used as

an alternative to CABG, coronary artery bypass grafting. CABG is an invasive procedure that requires general anesthesia and opening the chest cavity to perform the operation.

Depending on the location of obstruction or obstructions we recognize several clinically relevant classifications of CAD.

#### **Left main CAD**

Left main coronary artery supplies blood to 75–100% of the myocardium, making the obstructions at that site exceptionally high risk, see [5].

#### **Multivessel CAD**

Includes involvement of at least two of the following 3 major arteries: left anterior descending (LAD) artery, the left circumflex (LCx) artery, and the right coronary artery (RCA), see [6]. One-vessel and two-vessel CAD are analogously defined.

#### **Proximal LAD involved in multivessel, one-vessel or two-vessel CAD**

Involvement of proximal LAD represents greater risk because LAD supplies blood to 40–50% of left ventral myocardium. Proximal refers to proximity to the branching point of left main coronary artery.

Terminology surrounding CAD related syndromes was subject to change. Previously, CAD related syndromes were classified as stable or acute. In 2019, European Society of Cardiology replaced the term stable CAD with chronic coronary syndrome. Term stable CAD implies predictable progression of disease or dormancy of pathological process underlying the disease. Term chronic coronary syndrome was introduced to reflect current understanding of CAD as a dynamic process that can have long stable periods but can also become unstable at any time. Most common disruption of stability is acute atherothrombotic event caused by plaque rupture or erosion, see [7].

### **Chronic coronary syndromes**

2024 ESC (European Society of Cardiology) Guidelines for the diagnosis and management of chronic coronary syndromes introduced the following definition of the term:

”Chronic coronary syndromes (CCS) are a range of clinical presentations or syndromes that arise due to structural or functional alterations related to chronic diseases of the coronary arteries or microcirculation. These alterations can lead to transient, reversible, myocardial demand vs. blood supply mismatch resulting in hypoperfusion (ischemia), usually (but not always) provoked by exertion, emotion or other stress, and may manifest as angina, other

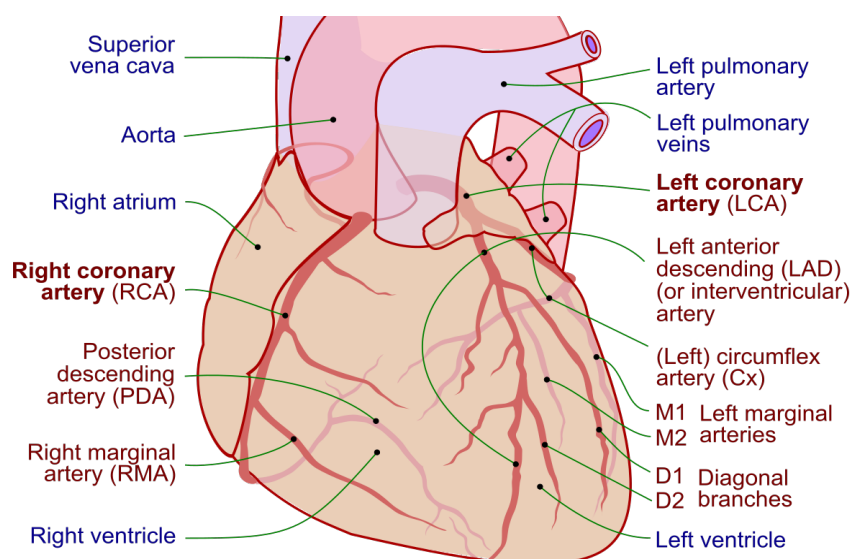


Figure 1.6: Coronary arteries. Patrick J. Lynch, medical illustrator derivative work: Fred the Oyster adaption and further labeling: Mikael Häggström, M.D. Link, accessed on 26.9.2024.

chest discomfort, or dyspnoea, or be asymptomatic. Although stable for long periods, chronic coronary diseases are frequently progressive and may destabilize at any moment with the development of an acute coronary syndrome (ACS).” See [6].

According to [6], the following CCS patients seek medical attention in clinical practice:

1. symptomatic patient with reproducible stress-induced angina or ischemia with epicardial obstructive CAD,
2. patient with angina or ischemia caused by epicardial vasomotor abnormalities or functional/structural microvascular alterations in the absence of epicardial obstructive CAD,
3. non-acute patient post-acute coronary syndrome or after a revascularization,
4. the non-acute patient with heart failure of ischemic or cardiometabolic origin,
5. asymptomatic individuals in whom epicardial CAD is detected during an imaging test.

Revascularization to improve outcomes or symptoms in CCS patients is becoming a more common practice. Our interest lies in percutaneous coronary intervention (PCI) with implantation of drug eluting stent (DES). Currently, revascularization by PCI is recommended or should be considered, see [6], for following patients:

**1. Left main disease**

CABG is preferred mode of revascularization for complex left main coronary artery stenosis. For CCS patients with significant left main coronary artery stenosis of low complexity PCI is preferred, and in case of intermediate complexity should be considered, because it is less invasive.

**2. Left main with multivessel disease**

CABG is recommended over medical therapy alone. PCI should be considered in patients with high surgical risk.

**3. Multivessel disease and diabetes**

In patients with insufficient response to medical therapy, CABG is recommended. In case of very high surgical risk, PCI should be considered.

**4. Three-vessel disease, without diabetes**

In patients with preserved left ventricular systolic function, insufficient response to medical therapy and significant stenosis of low to intermediate complexity PCI is recommended over CABG.

**5. Single- or double-vessel disease involving the proximal LAD**

In patients with insufficient response to medical therapy, CABG or PCI is recommended over medical therapy alone.

**6. Single- or double-vessel disease not involving the proximal LAD** In symptomatic patients with significant obstruction and insufficient response to medical therapy, PCI is recommended.

## **Acute coronary syndromes**

Acute coronary syndromes (ACS) are associated with a broad range of clinical presentations. Patients can be symptom free at presentation, have mild symptoms like chest discomfort or telltale symptoms like cardiac arrest, electrical/haemodynamic instability, or cardiogenic shock. Patients presenting with suspected ACS may eventually receive a diagnosis of acute myocardial infarction or unstable angina. Acute myocardial infarction is myocardial necrosis resulting from acute obstruction of a coronary artery. Unstable angina is defined as myocardial ischemia at rest or on minimal exertion in the absence of acute

cardiomyocyte injury/necrosis. Both conditions require emergent medical care, see [8].

The first step in treating the patient with suspected ACS is obtaining an electrocardiogram (ECG), a test that records the electrical signals in the heart. Presence of ECG patterns that are associated with myocardial infarction indicate a higher risk of immediate, life-threatening complications. Such patient requires emergent reperfusion. Ideally, patient should undergo primary PCI, that is immediate angiography followed by PCI as needed. Time is of the essence and if PCI can not be performed within 120 minutes after obtaining pathological ECG, fibrinolysis should be initiated. Here fibrinolysis refers to administering drugs that dissolve blood clots. If patient does not stabilize 60-90 min after administration of fibrinolytic agents rescue PCI needs to be performed, see [8].

Patients without such patterns on ECG, but with ongoing ischemic symptoms also face immediate risks, including ventricular arrhythmias. Severity of risk is assessed by medical professional. Very high risk patients are recommended to undergo an immediate invasive strategy with emergency angiography and PCI as needed, see [8].

## 1.4 PCI and stent implantation

Goal of the majority of PCI procedures is to dilate coronary artery obstructed by stenosis, or open an occluded one and then implant a stent. PCI is minimally invasive procedure and general anesthesia is not required. Patients are usually given light sedation, most commonly benzodiazepines and opioids such as fentanyl. Arterial access usually involves right radial artery or right femoral artery via arterial sheath, see [9].

With help of X-ray imaging catheter is advanced until the tip is at the ostium of the coronary artery. Catheter serves as channel to inject radiographic contrast, measure arterial pressure and introduce equipment into obstructed artery. A fine guidewire is advanced into the coronary artery and steered across the stenosis to be treated. All subsequent equipment is introduced by the guidewire. Next, balloon is guided to affected site and inflated in the stenosis to enlarge the lumen. After it is deflated and withdrawn, balloon with stent in collapsed form is introduced and inflated to expand stent struts against the arterial wall. All equipment, except stent, is withdrawn and a compression device is positioned over the puncture.

## 1.5 Pharmacological component of PCI and DES

Following subsections are largely based on an article by Khan and Ludman, see [9].

## **Evolution of PCI and accompanying pharmacological treatment**

Before stents were introduced in 1990s, PCI was performed in the same fashion as described in the previous section but without implantation of stent. The procedure is commonly referred to as balloon angioplasty. During balloon angioplasty, atheromatous plaque is squished and disrupted. Deep fissures extend into tunica media and allow blood to create a split between two layers of the vessel wall that can result in a loose flap of tissue. This, combined with prothrombotic elements released from the necrotic core, poses a great risk of acute vessel thrombosis, 5% in the first 24 h after procedure. Another risk is occurrence of re-stenosis during wound healing after procedure due to negative vessel remodeling and neo-intimal hyperplasia (cellular proliferation) with rates of 20-50%.

These problems were partially addressed with introduction of bare metal stents and antiplatelet agents. Stent provides structural support to the vessel wall, holds back dissection flaps and minimizes negative artery remodeling. Dual antiplatelet therapy (DAPT), typically a combination of aspirin and clopidogrel, was introduced to minimize stent thrombosis. Aspirin and clopidogrel metabolites irreversibly inhibit different signaling pathways involved in platelet activation and aggregation. Affected platelets are inhibited until their death (life cycle 7-10 days). DAPT is administered during the procedure and in the first few weeks after bare metal stent implantation, during wound healing. DAPT proved crucial in reducing stent thrombosis. Rates of acute vessel occlusion dropped to less than 1%. One problem remained unaddressed, namely neo-intimal hyperplasia that remained responsible for re-stenosis rate of 10-30% after the procedure.

Drug eluting stents (DES) were developed to address neo-intimal hyperplasia. DES normally consists of three components: stent platform, stent coating and therapeutic agent. Purpose of DES is to elute anti-proliferative drugs into the vessel wall for a few weeks after implantation to battle exaggerated proliferation of smooth muscle cells at the site of the wound. Re-stenosis rate dropped to around 5%. One serious complication caused by use of DES instead of bare metal stent was late stent thrombosis. Bare metal stent becomes covered by endothelium in 3-4 weeks after implantation and does not pose a high risk for thrombosis, so DAPT can be discontinued. In case of drug eluting stent endothelialization does not occur rapidly due to lack of proliferative response and DAPT must be prolonged.

DES struts can remain uncovered for long periods of time. Polymers used for coating in early DES sometimes induced inflammatory response and this resulted in stent thrombosis occasionally occurring much later after stent implantation than previously observed. Current DES have significantly better long-term safety profile mostly because of changes in design. They have thinner stent struts and more inert or absorbable polymer coating, which may be restricted to the stent's abluminal surface. Late stent thrombosis rates for

current DES are less than 1% at 6 years and less than those with bare metal stents.

### **Antiproliferative drugs used in DES**

First generation of drug eluting stents was marked by Cypher, sirolimus eluting stent and Taxus, paclitaxel eluting stent. Later generations of stents more commonly use everolimus, zotarolimus and biolimus A9, all part of limus family-related drugs that sirolimus is also a part of. All mentioned drugs are antiproliferative, but paclitaxel and limus-family drugs have different mechanisms of action, see [10].

Limus-family drugs form a complex with the cytoplasmic protein FKBP12. Complex then binds to mTORC1, a crucial protein involved in protein synthesis, cell growth, cell proliferation and angiogenesis. This binding inhibits mTORC1. Inhibition of mTORC1 leads to the arrest of the cell cycle in G1 phase of interphase, preventing proliferation. Inhibition of mTORC1 also impairs activation of downstream targets that are essential for protein synthesis and growth. Effect is inhibited cell growth. Cells are unable to grow or proliferate and eventually undergo apoptosis, see [11].

# Chapter 2

## Drug eluting stents

As mentioned before DES normally consists of three components: stent platform, stent coating and therapeutic agent. In this chapter we will focus on versatile DES designs. Stent platform is interesting to us because we want to study how different geometries effect the distribution of therapeutic agent in the vessel wall. Differing coating materials and modes of application greatly influence elution of therapeutic agent from DES. Properties of the therapeutic agent should also be known. Interaction of therapeutic agent with receptors on extracellular matrix and inside the cells greatly affects the concentration of free therapeutic agent in the tissue. The concentration of free therapeutic agent in the tissue in turn modulates the elution from DES coating, making the two processes interdependent.

### 2.1 Stent platform and geometry

Design of stent platform is crucial for both immediate and long term clinical outcomes. Poorly designed stents can cause artery injury, dissection and thrombosis. Stent platforms are typically made from biologically inert metals. First generation of stents was predominantly made from stainless steel. In recent years metallic alloys like cobalt–chromium, nickel–titanium and platinum–chromium are most commonly used since they allow for thinner stent struts and are more biologically inert than stainless steel, see[10]. Problems associated with first generation of DES, primarily late state thrombosis, also inspired use of more biologically based materials including fully biodegradable stents.

Stent geometries wildly vary. Some designs feature cylindrical or flat wires covered by a thin film of polymer coating, some feature flattened wires with holes filled by polymer coating.

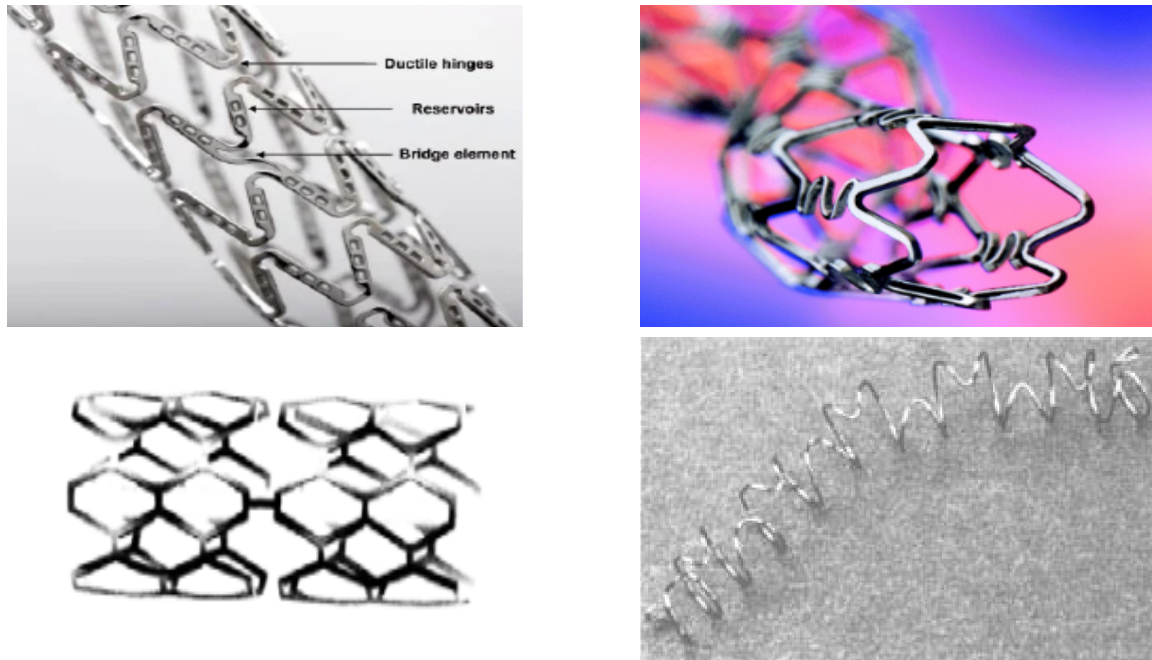


Figure 2.1: On the left and up we can see NEVO stent (Cordis), see [12]. Right up we can see CYPHER stent (Cordis), left down PALMAZ-SCHATZ stent (Johnson&Johnson), right down GIANTUCO-ROUBIN stent (Cook Inc.), see [13].

## 2.2 Stent coating

Stent platform is surrounded by polymer matrix containing drug. Polymers bind drug to the stent and modify elution of the drug. Surface characteristics of stent coating influence thrombosis and neointimal hyperplasia. Polymer should be haemocompatible to avoid thromboembolic processes. It should not flake or crack during any stage of DES delivery and deployment. Polymer also needs to be compatible with drug and be able to deliver the drug at a sustained, controlled and predictable rate.

Polymers used for coating stents can be broadly classified into biostable i.e permanent polymers, biodegradable polymers and biological polymers. Permanent polymers show best drug adhesion and delivery from stent but are associated with impaired vascular healing due to constant presence of polymer. In order to overcome these limitations, more biocompatible polymers with reduced potential for inflammatory response and delayed arterial healing were developed, see [10]. Today biocompatible permanent polymers are most commonly used.

Antiproliferative drugs, i.e. therapeutic agents, used in DES typically have low solubility in water. Densely packing such therapeutic agent in polymer matrix can improve bioavailability. Polymer matrix also modulates dissolution of therapeutic agent and restricts the amount of drug available for dissolution. Steady, i.e. controlled, release over long time period can be achieved, as discussed in [14].

The solubility profile of drug entrapped in polymer affects the controlled release.

1. Encapsulating a highly insoluble drug inside the polymer can end up with most of the drug on the outer layer of the polymer. In such cases "burst" kinetics, i.e. sudden release of large amount of drug followed by slow sustained release of drug, can be observed.
2. If highly insoluble drug is carefully compounded to be distributed in very small particles through the entire thickness of the polymer matrix release will follow Higuchi kinetics when exposed to perfect sink conditions. Higuchi kinetics will be discussed in the next chapter. Such release is linear in square root time.

Zero order release, i.e. release that is constant with time is usually wanted. There is no obvious solubility/diffusion profile that can deliver such release so devices have to be more complex. One of the ways this can be achieved is to choose polymer matrix that has outer layer in which saturated solubility of the drug is low and the concentration of drug in the inner part of the matrix is high, see [14]. In this case the outer layer of polymer matrix acts as a barrier that modulates elution of the drug.

## **Drug release from DES**

Success of stent implantation directly relies on effective delivery of therapeutics to the target site in biologically active form at prescribed concentration for sufficient amount of time. Release kinetics, mechanism of drug release and applied dose play a crucial role in determining duration and magnitude of arterial drug uptake.

In vitro experiments have been developed to simulate dissolution conditions mimicking the physiological situation at the site of implantation. In vitro release and experimentally derived distribution of drug can be modeled mathematically. Combined with use of finite element method (FEM) we can simulate drug release and distribution in the artery. Computational studies on drug elution from stents proved to be useful tool to optimize stent design and give insight into pharmacokinetics of drug delivery via DES.

Modelling of drug release from DES poses two challenges. Firstly, we must couple different models with possible singular behavior. Secondly, stents commonly have complex geometries that are taxing on computational resources/time. In next section we take a look at model proposed in [15].

# Chapter 3

## Model of controlled drug release

### 3.1 3D model of controlled drug release

We want to couple drug dissolution and release from DES with drug diffusion and transport in the artery. In this section we take a look at the model proposed by D'Angelo, Zunino, Porpora, Morlacchi and Migliavacca in [15].

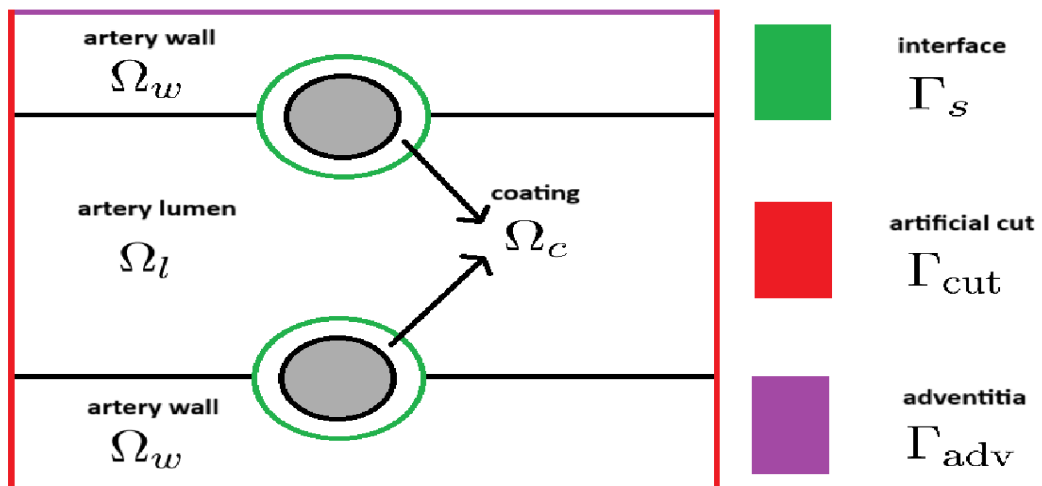


Figure 3.1: A sketch representing slice through an artery with 2 stent struts embedded in its wall, with an indication of domains and boundaries for problems. Dimensions are not adequately represented, the sketch serves only as a simplified representation of domains and boundaries. Gray area represents stent strut wire and is not a part of the domain.

## Domain

The domain is split into  $\Omega_c$ , representing coating surrounding the stent, and  $\Omega_a$  that represents artery as union of lumen  $\Omega_l$  and arterial wall  $\Omega_w$ . Boundary of  $\Omega_a$  can be split into  $\Gamma_s$  i.e. interface between coating and artery,  $\Gamma_{cut}$  representing artificial section and  $\Gamma_{adv}$  that represents outer wall tissue called adventitia. We also define  $\mathbf{n}_a$  as unit normal vector to  $\Omega_a$  and  $\mathbf{n}$  unit normal vector to  $\Gamma_s$  oriented towards the artery.

## Diffusion/dissolution model on $\Omega_c$

We assume that drug release from DES is controlled by drug dissolution and diffusion. Model proposed by Frenning, see [16], consists of two phase model for drug dissolution (solid and dissolved drug), and diffusion accounting for finite dissolution rate. We assume that drug does not chemically interact with the substrate.

Let  $\hat{s}$ ,  $\hat{c}$  be concentrations of solid and dissolved drug in the coating. Let  $c_s$  be saturation level of drug dissolved in water. We will use nondimensional concentrations  $s = \hat{s}/c_s$  and  $c = \hat{c}/c_s$  for modelling. Dissolution rate is governed by Nernst–Brunner equation, see [17]. Nernst–Brunner equation correlates the dissolution rate of solid drug and concentration gradient i.e. the difference in the concentration of drug solution at the solid drug surface and in the bulk solution. Let the layer of dissolved drug surrounding exposed surface have thickness  $h$ . Letting  $V$  be volume of bulk solution,  $S$  exposed surface of solid drug, and  $D_c$  diffusion coefficient of drug in solute. Then the evolution of the solid drug is described by the following equation

$$\frac{d\hat{s}}{dt} = -\frac{D_c S}{h V}(c_s - \hat{c}).$$

To take a closer look we also consider formulation proposed in [18]. Let  $w$  be amount, i.e. mass, of solid drug in the coating. Proposed formulation is

$$\frac{dw}{dt} = -K_2 S(c_s - \hat{c}).$$

Since  $\hat{s} = w/V$  we obtain the following

$$\frac{d\hat{s}}{dt} = -K_2 \frac{S}{V}(c_s - \hat{c}).$$

Obviously, formulations are equivalent and  $K_2 = D_c/h$ . For a solid substance whose crystals do not change shape i.e. only shrink in size during dissolution process, it is possible to express  $S$ , area of exposed surface of solid, as a function of  $w$ , the amount of the remaining

solid drug. In order to derive this function, we conceptualize solid drug dispersed in the polymer matrix as spherical particles, uniformly arranged in the grid as shown in Figure 3.2.

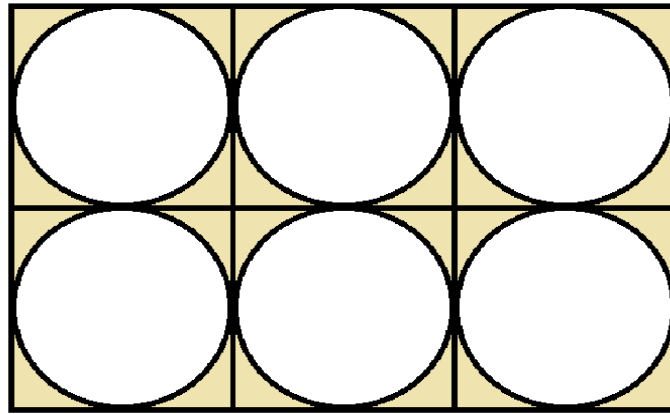


Figure 3.2: A sketch representing cross-section through the coating i.e. polymer matrix containing drug. Spherical particles are embedded in cubes that form a grid.

Density of drug in particles,  $d$ , is constant. Volume of particles decreases during the dissolution process. Let  $v(t)$  be volume of solid drug in the coating, and  $w(t)$  mass of solid drug in the coating, at time  $t$ . We have

$$v(t) = \frac{w(t)}{d}.$$

Since we assume that particles do not change shape, their surface and volume are determined by their radius  $r(t)$  at given time, with

$$S(t) = N \cdot 4\pi r(t)^2, \quad v(t) = N \cdot \frac{4}{3} r(t)^3,$$

where  $N$  is the number of particles in the coating. Next, we express  $S$  as function of  $w$ .

$$\begin{aligned}
S(t) &= 4N\pi \left( \frac{4}{3} N\pi r(t)^3 \right)^{2/3} \left( \frac{4}{3} N\pi \right)^{-2/3} \\
&= 4N\pi \left( \frac{4}{3} N\pi \right)^{-2/3} v(t)^{2/3} \\
&= 4N\pi \left( \frac{4}{3} N\pi \right)^{-2/3} d^{-2/3} w(t)^{2/3}.
\end{aligned}$$

For convenience we set  $k_s = 4N\pi \left( \frac{4}{3} N\pi \right)^{-2/3} d^{-2/3}$ , and obtain  $S(t) = k_s w(t)^{2/3}$ . Now we can return to equation  $\frac{dw}{dt} = -K_2 S (c_s - \hat{c})$  and substitute  $S$  with obtained formula.

$$\begin{aligned}
\frac{dw}{dt} &= -K_2 k_s w^{2/3} (c_s - \hat{c}), \\
\frac{d\hat{s}}{dt} &= -K_2 k_s V^{-1/3} \hat{s}^{2/3} (c_s - \hat{c}), && \text{(since } \hat{s} = w/V) \\
\frac{ds}{dt} &= -K_2 k_s V^{-1/3} c_s^{2/3} s^{2/3} (1 - c). && \text{(since } s = \hat{s}/c_s, c = \hat{c}/c_s)
\end{aligned}$$

Again, for convenience we set  $K = K_2 k_s V^{-1/3} c_s^{2/3}$ .

## MODEL

Model that describes amount of solid and dissolved drug in the coating is governed by dissolution of solid drug and Fickian diffusion of dissolved drug through the coating.

$$\begin{cases}
\partial_t c - \nabla \cdot (D_c \nabla c) = K (s^+)^{2/3} (1 - c) & \text{in } \Omega_c \times \mathbb{R}^+, \\
\partial_t s = -K (s^+)^{2/3} (1 - c) & \text{in } \Omega_c \times \mathbb{R}^+, \\
s = s_0, \quad c = 0 & \text{in } \Omega_c \times \{t = 0\}
\end{cases}$$

## PARAMETERS OF THE MODEL

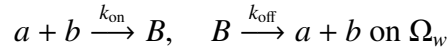
- $K > 0$  ~ dissolution constant
- $D_c > 0$  ~ diffusion coefficient

## Transport of drug into artery model on $\Omega_a$

Drug released to artery wall can assume 2 states. First state is drug dissolved in plasma in intercellular space. Second state is drug binding to receptors on extracellular matrix.

Artery lumen i.e. blood has no receptors and we do not consider it here.

Let  $a$  be concentration of drug in plasma permeated intercellular space,  $b$  density of free receptors,  $b_0$  their initial density and  $B$  concentration of drug attached to receptors. We assume that drug attached to receptors can no longer diffuse or be transported by plasma. Using mass conservation principle we have  $B = b_0 - b$ . Interaction between dissolved drug and receptors can be described by



where  $k_{\text{on}}, k_{\text{off}}$  are association and dissociation constants. Due to mass action law, rate of change for  $b$  is given by  $k_{\text{on}}ab + k_{\text{off}}(b - b_0)$ . Model for concentration of free and bound drug in the artery is governed by diffusion and interaction of drug with receptors.

MODEL

$$\begin{cases} \partial_t a - \nabla \cdot (D_a \nabla a) + k_{\text{on}}ab + k_{\text{off}}(b - b_0) = 0 & \text{in } \Omega_a \times \mathbb{R}^+, \\ \partial_t b + k_{\text{on}}ab + k_{\text{off}}(b - b_0) = 0 & \text{in } \Omega_a \times \mathbb{R}^+, \\ a = a_0(\mathbf{x}), \quad b = b_0(x) & \text{in } \Omega_a \times \{t = 0\}, \\ a = 0 & \text{on } \Gamma_{\text{adv}} \times \mathbb{R}^+, \\ \nabla a \cdot \mathbf{n}_a = 0 & \text{on } \Gamma_{\text{cut}} \times \mathbb{R}^+ \end{cases}$$

PARAMETERS OF THE MODEL

- $D_a > 0$  ~ diffusion coefficient in artery wall
- $k_{\text{on}}, k_{\text{off}} > 0$  ~ association and dissociation constants

BOUNDARY CONDITIONS

- $\Gamma_{\text{adv}}$  is well perfused and drug is washed out instantly
- on  $\Gamma_{\text{cut}}$  drug concentrations unperturbed if located far enough from  $\Gamma_s$

**Transmission conditions between  $\Omega_c$  and  $\Omega_a$**

Concentration of drug in plasma and coating interact through the boundary. Concentration and the flux from both sides have to match,

$$c = a \text{ and } D_a \nabla a \cdot \mathbf{n} = D_c \nabla c \cdot \mathbf{n} \text{ on } \Gamma_s \times \mathbb{R}^+.$$

To solve this problem numerically, one must apply finite difference scheme in time along with finite element method in space domain. The extremely thin coating relative to the whole domain is a significant obstacle in the discretization of the domain.

### 3.2 Polymer coating - 1D domain

In [15] authors avoided the complication of discretization of extremely thin coating domain by approximating the coating, i.e. domain  $\Omega_c$ , as an indefinite slab. The domain  $\Omega_c$  is represented by the 1D interval  $x \in (0, L)$ , where  $L$  is the thickness of the coating. Here 0 represents inert inner boundary adjacent to stent wire and  $L$  represents outer boundary i.e. interface. One assumption is that initially all drug is loaded in solid phase,  $s_0 > 1$ , in an uniform fashion. They also restrict their analysis to the small diffusion regime. Central assumption is made about the concentration level  $a(t)$  at external medium of boundary located at  $x = L$ .

**Assumption 3.2.1.** *The external drug concentration  $a(t)$  is such that*

$$\max_t |\partial_t a(t)| = |\partial_t a(t=0)|;$$

*increments of  $a(t)$  are small i.e.  $|a(t) - a(0)| \ll t$ .*

The dynamics of such system can be split in two phases. In the first, short phase, evolution starts with a sharp decrease of the solid drug concentration from  $s = s_0$  to  $s = s_0 - 1$  and  $c = 0$  increases to almost 1. Without the influence of the external boundary,  $c$  and  $s$  would converge to  $c = 1$  and  $s = s_0 - 1$ . In this phase  $c = 1$  everywhere except in the neighborhood of the external boundary where concentration is fixed at  $a(t) < 1$ . Characteristic time of this phase is proportional to  $s_0^{1/3}$ .

In the second phase, system shifts to a stable equilibrium  $s(t) = 0$  and  $c(t) = a(t)$  at  $x = L$ . The highest drug concentration jump with respect to the saturation level is now located at  $x = L$ . Propagating front for the solid drug concentration  $s$  moves towards the inner part and leaves behind a region depleted of solid drug where  $c$  obeys a simple homogeneous diffusion equation.

To estimate parameters of the model for specific stent we have to look at in vitro and in vivo experimental studies. Estimating parameters proved to be a hard task because experimental studies, data and explicitly given parameters are scarce. In the next section we propose a way to obtain  $D_c$  i.e. diffusivity of drug in the polymer coating by utilizing in vitro experimental studies on DES that maintain perfect sink conditions in combination with Higuchi's equation.

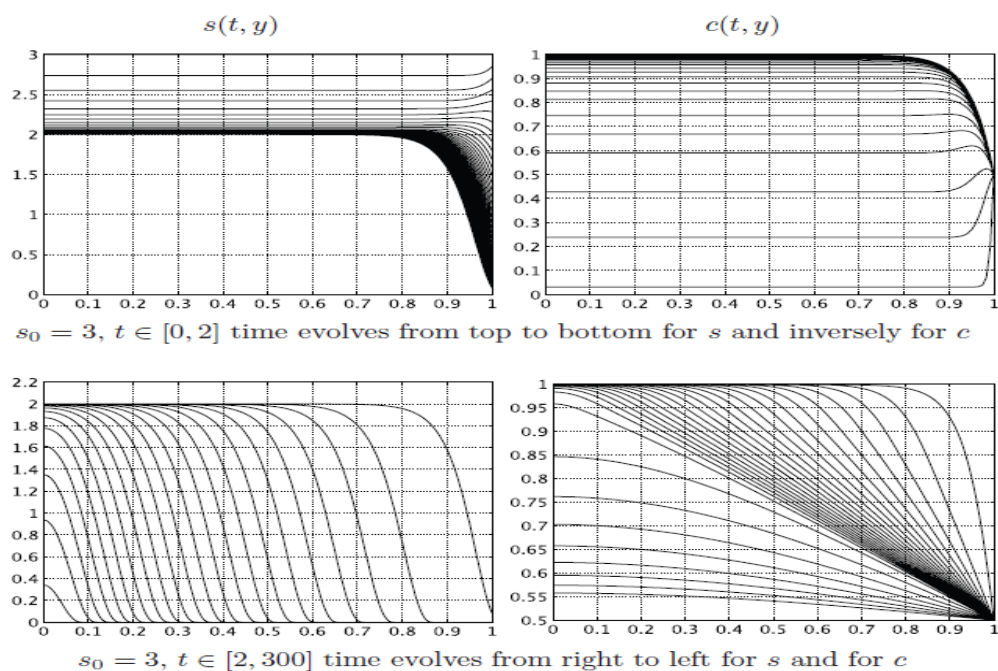


Figure 3.3: Numerical solutions of problem with model parameters, see [15]. Here  $1 = L$ .

### 3.3 Higuchi's equation - perfect sink conditions

In this section we take a look at study [19]. Authors obtained in vitro elution profile of sirolimus eluting stent over 24h and found that such elution profile mirrors 30 day in vivo porcine profile. The method has been accepted by the FDA as a release method for the elution of sirolimus in cardiovascular stents. Conditions in which experiment is conducted suggest perfect sink conditions at the stent-solvent interface. DES is placed in flow-trough cell containing 50 ml of bulk solution. Flow rate in experiment is 25 ml/min suggesting that drug eluted in bulk solution is quickly cleared.

Perfect sink conditions coupled with extremely thin coating of DES allow us to assume that mathematical model Takeru Higuchi proposed for release of a drug from a thin ointment film into the skin, see [20], can be applied. The model has 9 assumptions. In next 9 points we will access if Higuchi's assumptions fit the situation we are observing.

1. Drug transport through the film base is rate limiting. Drug transport within the skin is rapid.

*Drug release from DES is rate limiting. Drug transport in bulk solution is rapid, bulk solution is stirred.*

2. The skin acts like a “perfect sink”: The drug concentration in this compartment can be considered to be negligible.  
*Drug concentration in bulk solution is negligible compared to drug concentration in polymeric layer of DES.*
3. The initial drug concentration in the film is much higher than the solubility of the drug in the ointment base.  
*In DES concentration of sirolimus is multiple times higher than solubility of sirolimus in DES exposed to solvent.*
4. The drug is finely dispersed within the ointment base (the size of the drug particles is much smaller than the thickness of the film).  
*Our assumption is that the drug is finely dispersed and uniformly distributed throughout the film layer.*
5. The drug is initially homogeneously distributed throughout the film.  
*Assumption for our model is the same.*
6. The dissolution of drug particles within the ointment base is rapid compared to the diffusion of dissolved drug molecules within the ointment base.  
*Assumption for DES loaded with sirolimus is the same. Also initial drug load exceeds drug solubility multiple times, as is the case with DES loaded with sirolimus.*
7. The diffusion coefficient of the drug within the ointment base is constant and does not depend on time or the position within the film.  
*Our assumption is the same.*
8. Edge effects are negligible: The surface of the ointment film exposed to the skin is large compared to its thickness. The mathematical description of drug diffusion can be restricted to one dimension.  
*The polymeric coating on DES is extremely thin, when compared to stent strut thickness. The metallic component of the stent strut is the main contributor to the thickness. Consequently, surface of polymeric coating exposed to bulk solution is very large compared to its thickness.*
9. The medium (ointment base) does not swell or dissolve during drug release.  
*We assume that DES devices have durable polymer coating. Such coating maintains constant thickness and does not degrade during drug release.*

Drug molecules dissolved in the film diffuse into the skin under perfect sink conditions. The first phase is dominated by dissolution. Close to the skin-film interface drug dissolves and leaches into the skin. Drug dissolution is rapid and as long as large excess of drug is provided in this region particles that leach out of the film are rapidly replaced by dissolution of non dissolved particles in this region. In this short time span concentration near the skin-film interface is constant and equal to  $c_s$ . Dissolution of all solid particles in this region marks transition into the second phase, dominated by diffusion. Once there is no solid drug near the skin-film interface concentration in this region falls below saturation concentration  $c_s$ . Region that still contains solid drug is now further away from the skin-film interface. At the diffusion front, i.e. region that separates a layer of the film containing solid drug and a layer of the film that does not, concentration is maintained at  $c_s$ . Due to concentration gradient, dissolved drug particles located further away from the skin-film interface diffuse through the film base into the skin.

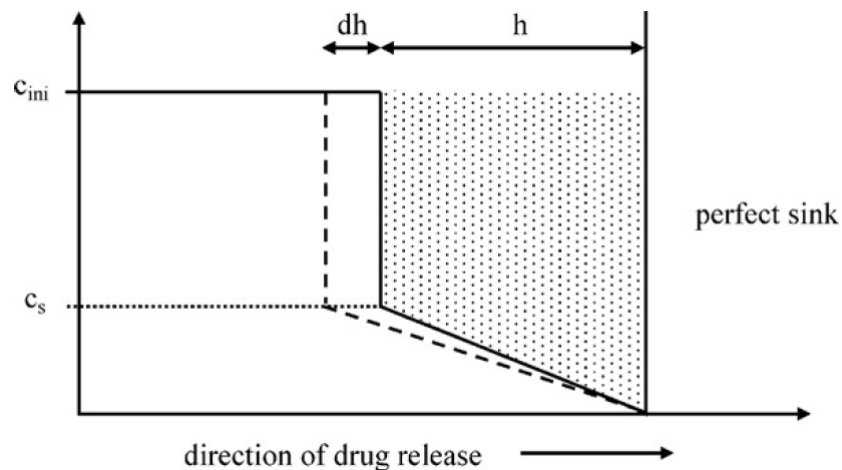


Figure 3.4: Graphic obtained from [20]. The drug concentration–distance–profile is represented by the solid line. y-axis represents the drug concentration, x-axis the distance. The diagram can be seen as a cross-section through the ointment film and the skin.  $c_{ini}$  is initial concentration of drug, higher than  $c_s$  the saturated concentration.

During the time in which solid drug is present in the film, pseudo-steady-state conditions are provided for drug diffusion. A saturated drug solution on the one side and a perfect sink on the other with a constant distance in-between. Using Fick's second law one can conclude that the amount of drug released from the film at time  $t$  can be represented by

dotted trapezoid in *Fig 1.*. Cumulative amount of drug released up until time  $t$  is therefore given by

$$M_t = A \cdot h \cdot \left( c_{\text{ini}} - \frac{1}{2} c_s \right),$$

where  $A$  is area of skin-film interface.

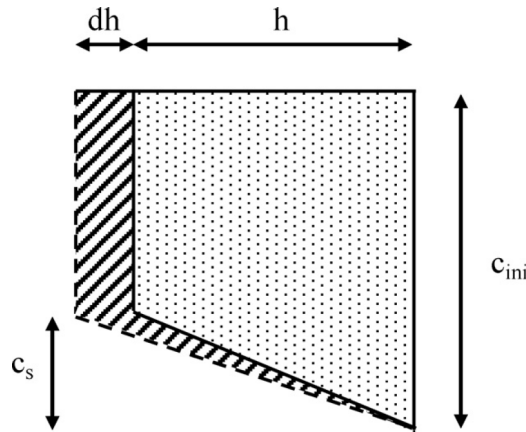


Figure 3.5: Graphic obtained from [20]. Cumulative amount of drug released up until time  $t$  represented by dotted trapezoid. Larger trapezoid (dotted + slashed area) represents cumulative amount of drug released up until time  $t + dt$ .

Cumulative amount of drug released  $dM_t/dt$  in the time interval  $dt$  is given by

$$\frac{dM_t}{dt} = A \cdot dh \cdot \left( c_{\text{ini}} - \frac{1}{2} c_s \right).$$

The Fick's 1st law of diffusion can also be used in order to quantify the amount of drug released from the ointment film in the time interval  $dt$ .

$$\frac{dM_t}{dt} = A \cdot D \cdot \frac{c_s}{h}.$$

Equating last two equations yields separable, first order, ordinary differential equation with solution

$$h(t) = 2 \sqrt{\frac{D \cdot c_s \cdot t}{2 \cdot c_{\text{ini}} - c_s}}.$$

From here we can obtain equation for  $M_t$ ,

$$M_t = A \cdot \sqrt{(2 \cdot c_{ini} - c_s) \cdot D \cdot c_s \cdot t},$$

and flux

$$J = \frac{1}{2} \sqrt{(2 \cdot c_{ini} - c_s) \cdot D \cdot c_s} \cdot \frac{1}{\sqrt{t}}.$$

Elution profile obtained in the experiment is linear in square time and Higuchi's equation for  $M_t$  can be used to fit the data and estimate parameter  $D$  i.e.  $D_c$  in proposed mathematical model, see [15]. Comparison between elution profile obtained in this in vitro experiment conforms very well to elution profile obtained from in vivo porcine studies, except at the first few time points, suggesting that even though Higuchi's equation can be utilized to study long term elution profile it is not an adequate tool to capture the entire elution profile.

In this study authors did not disclose specific type or types of DES used. It is not unreasonable to assume that stents in question were CYPHER or CYPHER Select, both sirolimus eluting stents with durable polymer coating, see [21]. Study was funded by Johnson&Johnson company, whose subsidiary Cordis manufactured and sold mentioned stents at that time (2011.). Picture of DES in apparatus used to measure the elution, included in the paper, further validates this assumption as the stent appears to be CYPHER, due to its geometry. Results of this study can be used to extract parameter  $D_c$  for sirolimus eluting stents featuring the same polymer matrix.

In the next section we take a look at in vivo experimental study, see [11]. To interpret obtained data authors combined Higuchi's equation and 1st order release kinetics to describe elution profile and achieved a more refined fit.

### 3.4 In vivo model

Study [11], examines how efficacy of DES depends on drug dose and elution duration. The study compared the arterial drug content achieved with two different sirolimus eluting stents. Stents used were the CYPHER Stent (Cordis Corporation, NJ) and a prototype of the NEVO Stent (Cordis Corporation, NJ). Used CYPHER stent has a radius of 3.5mm and length of 18mm. It has square wires, i.e. wires whose cross section can be roughly by a square, and is coated with two durable polymers containing sirolimus dose of 175g. NEVO stent (3.5mm x 17mm) has flat stent wires, i.e wires whose cross section can be well estimated by a narrow rectangle. Hundreds of discrete holes are drilled in stent scaffold and filled with biodegradable polymer containing 166g of sirolimus. In the study stented arteries were harvested 1, 3, 8, 14 and 30 days post-implantation and sirolimus content in both

artery and stent has been evaluated.

Authors idealized CYPHER coatings as 2 monolithic polymer films, each containing a pool of dispersed drug. The outer film contains surface connected drug that diffuses through the film and elutes through a percolating network of drug filled pores. Drug in the inner film is embedded within the matrix and diffuses more slowly through the percolating polymer phase. Assumption was made that the first pool of drug is eluted fast in comparison with the second pool of drug. It is modeled as first order process. Assumption about the second pool of drug is that it follows Higuchi type, diffusion limited, dissolution kinetics. Cumulative sirolimus elution kinetics from CYPHER coatings are parameterized in [11] as

$$M_{\text{stent}}(0) - M_{\text{stent}}(t) = M_{f_0} (1 - e^{-K_{f_0} t}) + Q_{\text{sus}} \sqrt{t}.$$

$M_{\text{stent}}(0)$  is initial load of drug in stent (g),  $M_{f_0}$  is the initial pool of first order eluting drug (g).  $K_{f_0}$  ( $\text{d}^{-1}$ ) and  $Q_{\text{sus}}$  ( $\text{g} \cdot \text{d}^{-1/2}$ ) are rate constants.

Sirolimus inhibits intimal hyperplasia by inhibiting mTOR signaling pathway. Sirolimus binds to intracellular protein FKBP12. Sirolimus bound protein FKBP12 binds to another protein, FRAP. This protein is essential for progression of the cell cycle from G1, phase of cell growth, to S phase, phase in which cell synthesizes a copy of nuclear DNA. Disturbance leads to arrest of cell cycle and eventual cell death. Sirolimus also binds to general ECM (extra cellular matrix) sites. To predict drug distribution in the artery and biological effects, binding to both specific receptors and general ECM sites must be accounted for. The following model is proposed.

$$\begin{aligned} \frac{\partial c}{\partial t} + \frac{\partial b_{\text{ECM}}}{\partial t} + \frac{\partial b_{\text{REC}}}{\partial t} &= D_{\text{wall}} \frac{\partial^2 c}{\partial r^2} + \frac{D_{\text{wall}}}{r} \frac{\partial c}{\partial r} - V_{\text{wall}} \frac{\partial c}{\partial r}, \\ \frac{\partial b_{\text{ECM}}}{\partial t} &= k_{\text{on}}^{\text{ECM}} c (b_{\text{ECM}, \text{max}} - b_{\text{ECM}}) - k_{\text{on}}^{\text{ECM}} K_{\text{d}}^{\text{ECM}} b_{\text{ECM}}, \\ \frac{\partial b_{\text{REC}}}{\partial t} &= k_{\text{on}}^{\text{REC}} c (b_{\text{REC}, \text{max}} - b_{\text{REC}}) - k_{\text{on}}^{\text{REC}} K_{\text{d}}^{\text{REC}} b_{\text{REC}}. \end{aligned}$$

Here  $r$  represents distance from the intima,  $c$  the molar concentration of free drug per unit tissue volume.  $b_{\text{REC}}$  and  $b_{\text{ECM}}$  are the molar concentrations of receptor and ECM bound drug.  $b_{\text{REC}, \text{max}}$  and  $b_{\text{ECM}, \text{max}}$  represent local molar concentration of receptor and ECM drug binding sites.  $k_{\text{on}}^{\text{REC}}$  and  $k_{\text{on}}^{\text{ECM}}$  are binding/association rate constants.  $K_{\text{d}}^{\text{REC}}$  and  $K_{\text{d}}^{\text{ECM}}$  equilibrium dissociation constants.  $D_{\text{wall}}$  is the transmural diffusivity of the drug and  $V_{\text{wall}}$  is its transmural convective velocity. Notice that  $k_{\text{off}}$  parameter in model proposed in [15] is equivalent to  $K_{\text{d}}^{\text{REC}} \cdot k_{\text{on}}^{\text{REC}}$  and  $K_{\text{d}}^{\text{ECM}} \cdot k_{\text{on}}^{\text{ECM}}$ .

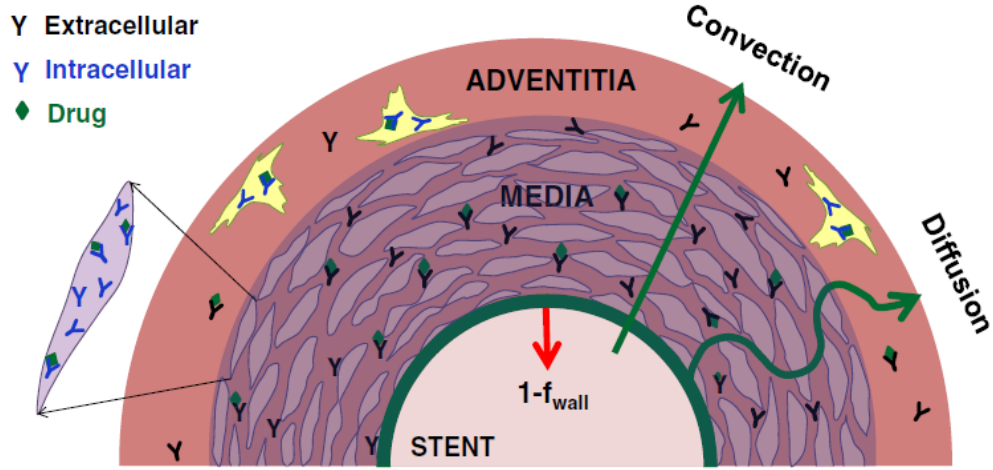


Figure 3.6: Graphic obtained from [11]. DES is idealized as phantom interface separating arterial tissue from luminal blood, delivering fraction  $f_{\text{wall}}$  of drug to luminal wall while the remaining fraction is cleared by luminal blood.

The authors neglected actual geometry of the stent and idealized stent as phantom interface. Fraction  $f_{\text{wall}}$  of drug is delivered to the luminal wall, the remainder is cleared by luminal blood. Elution from the phantom surface is modeled by prescribed luminal and wall fluxes that are proportional to the in vivo net flux. Boundary conditions are as follows:

$$D_{\text{wall}} \frac{\partial c}{\partial r} - V_{\text{wall}} c = f_{\text{wall}} \frac{dM_{\text{stent}}}{dt} \cdot (S_{\text{lumen}} \cdot A_{\text{drug}}), \quad \text{on } r = r_{\text{min}} \text{ (interface)}$$

$$c = 0, \quad \text{on } r = r_{\text{min}} + W \text{ (adventitia)}$$

In order to compare experimental results with the model, relationship between drug elution rate and the total drug content per tissue weight is utilized.

$$C_{\text{tissue}}(t) = \frac{A_{\text{drug}}}{W \rho_{\text{tissue}}} \int_{r_{\text{min}}}^{r_{\text{min}}+W} [c(t) + b_{\text{ECM}}(t) + b_{\text{REC}}(t)] dr$$

Here  $\rho_{\text{tissue}}$  is the density of wet arterial tissue. In vivo inhibition of mTOR signaling pathway by sirolimus is estimated using average fraction of bound FKBP12.

$$\text{Fractional effect } (t) = \frac{1}{W} \int_{r_{\text{min}}}^{r_{\text{min}}+W} \frac{b_{\text{REC}}(r, t)}{b_{\text{REC, max}}} dr$$

CYPHER stents exhibited biphasic elution kinetics, compatible with 42.4% of the initial load eluting at a fast first order rate and the rest eluting by diffusion-limited dissolution.

Study found that the rate of adventitial sirolimus clearance exceeds the rate of sirolimus absorption at the interface. Implication is that sirolimus traverses the full thickness of the arterial wall within 24 h of stenting.

In the study all parameters are either taken from literature or estimated by numerical means using experimental results in frame of presented mathematical model. The study gives us a useful insight about behavior of sirolimus eluting stents and a toolbox to interpret results of numerical simulations in a way that is applicable in clinical practice. We will use parameters from this study directly. We will also use information about dimension of Cypher stent and initial loading of sirolimus in Cypher stent, in conjunction with data from [19] to estimate parameter  $K$ .

### 3.5 2D model for controlled drug release

In this section we adapt model from section 3.1. to incorporate 2 different pools of receptors drug can bind to, as in [11]. We also restrict our model to 2D domain.

#### Domain sketch

We consider restriction of model [15] to 2D domain. We idealize stent struts and consider that the entire stent strut is made of polymer coating. We expect the concentration of solid and dissolved drug in the coating to follow the behaviour outlined in section 3.2, in which case the surplus of drug in the domain does not disrupt dynamics of elution from the stent, and instead only prolongs it.

We derive domain from 3D model in the following way.  $\Omega_w$  is intersection of closure of the artery wall domain and the artery lumen domain without closure of the coating domain. Cross section in line with derived  $\Omega_w$  is made through the stent strut to derive domain  $\Omega_c$ .  $\Gamma_s$  and  $\Gamma_{cut}$  are as depicted in the graphic. Incision  $\Gamma_{flat}$  is made along the artery allowing us to "unroll" the domain into the flat surface. To compensate for making such incision we demand that all functions defined on the domain  $\Omega_w$  and  $\Omega_c$  be periodic with respect to  $\Gamma_{flat}$ .

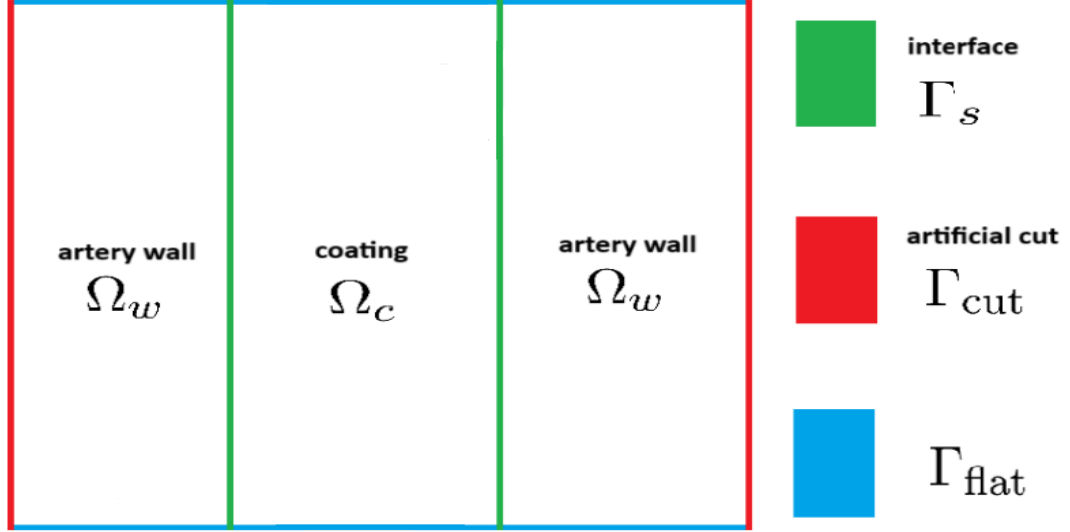


Figure 3.7: A sketch of single stent wire laying on the arterial wall, with an indication of domains and boundaries for problems.

#### Diffusion/dissolution model on $\Omega_c$

Diffusion/dissolution model translates directly from [15] to 2D domain.

$$\begin{cases} \partial_t c - \nabla \cdot (D_c \nabla c) = K (s^+)^{2/3} (1 - c) & \text{in } \Omega_c \times \mathbb{R}^+, \\ \partial_t s = -K (s^+)^{2/3} (1 - c) & \text{in } \Omega_c \times \mathbb{R}^+, \\ s = s_0, \quad c = 0 & \text{in } \Omega_c \times \{t = 0\} \end{cases}$$

#### Transport of drug into artery model on $\Omega_w$

We want to model transport of drug into artery wall. We omit effect plasma filtration in the artery wall has on transport and consider that drug binds to two different pools of receptors.

$$\begin{cases} \partial_t a - \nabla \cdot (D_a \nabla a) - \partial_t b_R - \partial_t b_E = 0 & \text{in } \Omega_w \times \mathbb{R}^+, \\ \partial_t b_R + k_{\text{on}}^R a b_R + k_{\text{off}}^R (b_R - b_{R0}) = 0 & \text{in } \Omega_w \times \mathbb{R}^+, \\ \partial_t b_E + k_{\text{on}}^E a b_E + k_{\text{off}}^E (b_E - b_{E0}) = 0 & \text{in } \Omega_w \times \mathbb{R}^+, \\ a = a_0(\mathbf{x}), \quad b_R = b_{R0}(\mathbf{x}), \quad b_E = b_{E0}(\mathbf{x}) & \text{in } \Omega_w \times \{t = 0\}, \\ \nabla a \cdot \mathbf{n}_a = 0 & \text{on } \Gamma_{\text{cut}} \times \mathbb{R}^+ \end{cases}$$

Here  $b_R$  is the density of free receptors sirolimus binds to, forming a complex that has inhibitory effect on neointimal hyperplasia.  $b_{R0}$  is their initial density.  $b_E$  represents density of free receptors sirolimus binds to, but such binding does not have any direct effect on neointimal hyperplasia.  $b_{E0}$  is their initial density. Association and dissociation constants  $k_{\text{on}}^E$  and  $k_{\text{off}}^E$  are equivalent to  $k_{\text{on}}^{\text{ECM}}$  and  $k_{\text{on}}^{\text{ECM}} K_d^{\text{ECM}}$ . Analogously,  $k_{\text{on}}^R$  and  $k_{\text{off}}^R$  are equivalent to  $k_{\text{on}}^{\text{REC}}$  and  $k_{\text{on}}^{\text{REC}} K_d^{\text{REC}}$ .

Transmission conditions

$$c = a \text{ and } D_a \nabla a \cdot \mathbf{n} = D_c \nabla c \cdot \mathbf{n} \text{ on } \Gamma_s \times \mathbb{R}^+$$

need to be satisfied.

### Weak formulation

In order to solve the coupled problem numerically using the finite element method, we must first find the weak formulation of the coupled problem. We will solve both problems simultaneously. For the finite element method discretization we use the tool called FreeFEM++ which requires that all unknown functions are defined on the same domain,  $\Omega = \Omega_w \cup \Omega_c$ . We define function  $c_{\text{all}}$ , concentration of dissolved drug on  $\Omega$ . The drug has different diffusion coefficient on  $\Omega_a$  and  $\Omega_c$ , so we define function  $D = D_a \cdot \chi_{\Omega_a} + D_c \cdot \chi_{\Omega_c}$ . Here  $\chi_{\Omega_c}, \chi_{\Omega_a}$  represent indicator functions of sets  $\Omega_c, \Omega_a$ . Such definition of concentration instantly satisfies transmission conditions in the weak formulation of the coupled problem.

$$\left\{ \begin{array}{ll} \partial_t c_{\text{all}} - \nabla \cdot (D \nabla c_{\text{all}}) - K(s^+)^{2/3} (1 - c_{\text{all}}) \chi_{\Omega_c} \\ \quad + k_{\text{on}}^R c_{\text{all}} b_R \chi_{\Omega_w} + k_{\text{off}}^R (b_R - b_{R0}) \chi_{\Omega_w} \\ \quad + k_{\text{on}}^E c_{\text{all}} b_E \chi_{\Omega_w} + k_{\text{off}}^E (b_E - b_{E0}) \chi_{\Omega_w} = 0 & \text{in } \Omega \times \mathbb{R}^+, \\ \partial_t s = -K(s^+)^{2/3} (1 - c_{\text{all}}) & \text{in } \Omega_c \times \mathbb{R}^+ \\ \partial_t b_R + k_{\text{on}}^R c_{\text{all}} b_R + k_{\text{off}}^R (b_R - b_{R0}) = 0 & \text{in } \Omega_w \times \mathbb{R}^+, \\ \partial_t b_E + k_{\text{on}}^E c_{\text{all}} b_E + k_{\text{off}}^E (b_E - b_{E0}) = 0 & \text{in } \Omega_w \times \mathbb{R}^+, \\ c_{\text{all}} = 0, \quad b_R = b_{R0}(x), \quad b_E = b_{E0}(x), \quad s = 0 & \text{in } \Omega_w \times \{t = 0\}, \\ c_{\text{all}} = 0, \quad b_R = 0, \quad b_E = 0, \quad s = s_0 & \text{in } \Omega_c \times \{t = 0\}, \\ \nabla c_{\text{all}} \cdot \mathbf{n}_a = 0 & \text{on } \Gamma_{\text{cut}} \times \mathbb{R}^+ \end{array} \right.$$

Note that  $b_R$  and  $b_E$  are meaningless in  $\Omega_c$ . We write them on  $\Omega_c$  for the purpose of addition in FreeFEM++. However their value in  $\Omega_c$  will not influence their value in  $\Omega_w$  since there are no space derivatives in equations for  $b_E$  and  $b_R$ . Similar holds for  $s$ . To obtain weak formulation we first multiply each equation with different test function and then integrate those equations on the whole space domain.

1. Multiplying the 1st equation with test function  $\omega_c$  and integrating over the domain  $\Omega$ .

$$\begin{aligned} \int_{\Omega} \partial_t c_{all} \omega_c - \int_{\Omega} \nabla \cdot (D \nabla c_{all}) \omega_c - \int_{\Omega} K(s^+)^{2/3} (1 - c_{all}) \chi_{\Omega_c} \omega_c \\ + \int_{\Omega} \left[ k_{on}^R c_{all} b_R + k_{off}^R (b_R - b_{R0}) + k_{on}^E c_{all} b_E + k_{off}^E (b_E - b_{E0}) \right] \chi_{\Omega_w} \omega_c = 0. \end{aligned}$$

Term  $\nabla \cdot (D \nabla c_{all}) \omega_c$  can be rewritten as

$$\nabla \cdot (D \nabla c_{all}) \omega_c = \nabla \cdot (D \nabla c_{all} \omega_c) - D \nabla c_{all} \cdot \nabla \omega_c.$$

Now the corresponding integral becomes

$$\begin{aligned} \int_{\Omega} \nabla \cdot (D \nabla c_{all}) \omega_c &= \int_{\Omega} \nabla \cdot (D \nabla c_{all} \omega_c) - \int_{\Omega} D \nabla c_{all} \cdot \nabla \omega_c \\ &= \int_{\partial \Omega} \omega_c D \nabla c_{all} \cdot \mathbf{n} - \int_{\Omega} D \nabla c_{all} \cdot \nabla \omega_c \quad (\text{Green's thm.}) \\ &= - \int_{\Omega} D \nabla c_{all} \cdot \nabla \omega_c \end{aligned}$$

Finally we obtain

$$\begin{aligned} \int_{\Omega} \partial_t c_{all} \omega_c + \int_{\Omega} D \nabla c_{all} \cdot \nabla \omega_c - \int_{\Omega} K(s^+)^{2/3} (1 - c_{all}) \chi_{\Omega_c} \omega_c \\ + \int_{\Omega} k_{on}^R c_{all} b_R \chi_{\Omega_w} \omega_c + \int_{\Omega} k_{off}^R (b_R - b_{R0}) \chi_{\Omega_w} \omega_c \\ + \int_{\Omega} k_{on}^E c_{all} b_E \chi_{\Omega_w} \omega_c + \int_{\Omega} k_{off}^E (b_E - b_{E0}) \chi_{\Omega_w} \omega_c = 0. \end{aligned}$$

2. Multiplying the 2nd equation with test function  $\omega_R$  and integrating over the domain  $\Omega$ .

$$\int_{\Omega} \partial_t b_R \omega_R = - \int_{\Omega} k_{on}^R c_{all} b_R \chi_{\Omega_w} \omega_R - \int_{\Omega} k_{off}^R (b_R - b_{R0}) \chi_{\Omega_w} \omega_R.$$

3. Multiplying the 3rd equation with test function  $\omega_E$  and integrating over the domain  $\Omega$ .

$$\int_{\Omega} \partial_t b_E \omega_E = - \int_{\Omega} k_{on}^E c_{all} b_E \chi_{\Omega_w} \omega_E - \int_{\Omega} k_{off}^E (b_E - b_{E0}) \chi_{\Omega_w} \omega_E.$$

4. Multiplying the 4th equation with test function  $\omega_s$  and integrating over the domain  $\Omega$ .

$$\int_{\Omega} \partial_t s \omega_s = - \int_{\Omega} K(s^+)^{2/3} (1 - c_{all}) \chi_{\Omega_c} \omega_s.$$

### Approximating solutions $c_{all}$ , $s$ , $b_R$ , $b_E$ at fixed time points

Let  $\Delta t$  be a fixed time step. Let  $t^n = n \cdot \Delta t$  for  $n \in 0, 1, \dots, N$ . We can approximate partial derivatives of  $c_{all}$ ,  $s$ ,  $b_E$  and  $b_R$  with respect to time at time  $t^n$  with

$$\begin{aligned}\frac{c_{all}(t^{n+1}) - c_{all}(t^n)}{\Delta t} &\approx \partial_t c_{all}(t^n), \\ \frac{s(t^{n+1}) - s(t^n)}{\Delta t} &\approx \partial_t s(t^n), \\ \frac{b_R(t^{n+1}) - b_R(t^n)}{\Delta t} &\approx \partial_t b_R(t^n), \\ \frac{b_E(t^{n+1}) - b_E(t^n)}{\Delta t} &\approx \partial_t b_E(t^n).\end{aligned}$$

Let  $c_{all}^n \approx c_{all}(t^n)$ ,  $s^n \approx s(t^n)$ ,  $b_R(t^n)$  and  $b_E(t^n)$  be approximations of corresponding functions at time  $t^n$ . Using the weak formulation of differential equations and initial values of functions at time  $t = 0$  we can approximate functions at next time step  $\Delta t$ . Repeating this process yields solutions for the next time steps.

In order to achieve greater stability of the numerical approximations, we implement Newton's type method at each time step. Instead of approximating  $c_{all}^{n+1}$  directly, we implement  $k$  iterations in which we approximate  $\Delta c_{all}$  where

$$c_{all}^{n+1,k+1} = c_{all}^{n+1,k} + \Delta c_{all}, \quad c_{all}^{n+1,0} = c_{all}^n.$$

In the last iteration we obtain  $c_{all}^{n+1} = c_{all}^{n+1,k} + \Delta c_{all}$ .

Identical method will be implemented for  $b_R$  and  $b_E$ . In the case of function  $s$  we have term  $(s^+)^{2/3}$ . In program we are utilizing for numerical approximation, FreeFEM++, this term is not differentiable. Therefore, our implementation of Newton's method will be only partial, and for this term we use just simple iterations.

Formulation of our problem that is compatible with FreeFEM++ solver is given on the next page. We ignore quadratic terms of type  $\Delta f_1 \cdot \Delta f_2$  where  $f_1, f_2$  are unknown functions of interest since their contribution is small. To simplify the notation, terms  $c_{all}^{old}$ ,  $b_R^{old}$ ,  $b_E^{old}$  and  $s^{old}$  represent known functions from previous time step. Terms  $c_{all}^0$ ,  $b_R^0$ ,  $b_E^0$  and  $s^0$  represent known initial values of functions at  $t = 0$ . In addition we sum the weak formulations of all equations from the previous page. Thus for all  $\omega_c$ ,  $\omega_E$ ,  $\omega_R$ ,  $\omega_s$  smooth enough the following equation holds.

$$\begin{aligned}
& \int_{\Omega} c_{all} \omega_c + \int_{\Omega} \Delta c_{all} \omega_c - \int_{\Omega} c_{all}^{old} \omega_c \\
& + \int_{\Omega} \Delta t D \nabla c_{all} \cdot \nabla \omega_c + \int_{\Omega} \Delta t D \nabla (\Delta c_{all}) \cdot \nabla \omega_c \\
& + \int_{\Omega} \Delta t k_{on}^R c_{all} b_R \omega_c \chi_{\Omega_w} + \int_{\Omega} \Delta t k_{on}^R \Delta c_{all} b_R \omega_c \chi_{\Omega_w} + \int_{\Omega} \Delta t k_{on}^R c_{all} \Delta b_R \omega_c \chi_{\Omega_w} \\
& + \int_{\Omega} \Delta t k_{off}^R b_R \omega_c \chi_{\Omega_w} + \int_{\Omega} \Delta t k_{off}^R \Delta b_R \omega_c \chi_{\Omega_w} - \int_{\Omega} \Delta t k_{off}^R b_{R0} \omega_c \chi_{\Omega_w} \\
& + \int_{\Omega} \Delta t k_{on}^E c_{all} b_E \omega_c \chi_{\Omega_w} + \int_{\Omega} \Delta t k_{on}^E \Delta c_{all} b_E \omega_c \chi_{\Omega_w} + \int_{\Omega} \Delta t k_{on}^E c_{all} \Delta b_E \omega_c \chi_{\Omega_w} \\
& + \int_{\Omega} \Delta t k_{off}^E b_E \omega_c \chi_{\Omega_w} + \int_{\Omega} \Delta t k_{off}^E \Delta b_E \omega_c \chi_{\Omega_w} - \int_{\Omega} \Delta t k_{off}^E b_{E0} \omega_c \chi_{\Omega_w} \\
& - \int_{\Omega} \Delta t K(s^+)^{2/3} \omega_c \chi_{\Omega_c} + \int_{\Omega} \Delta t K(s^+)^{2/3} c_{all} \omega_c \chi_{\Omega_c} + \int_{\Omega} \Delta t K(s^+)^{2/3} \Delta c_{all} \omega_c \chi_{\Omega_c} \\
& + \int_{\Omega} b_R \omega_R + \int_{\Omega} \Delta b_R \omega_R - \int_{\Omega} b_R^{old} \omega_R \\
& + \int_{\Omega} \Delta t k_{on}^R c_{all} b_R \omega_R \chi_{\Omega_w} + \int_{\Omega} \Delta t k_{on}^R \Delta c_{all} b_R \omega_R \chi_{\Omega_w} + \int_{\Omega} \Delta t k_{on}^R c_{all} \Delta b_R \omega_R \chi_{\Omega_w} \\
& + \int_{\Omega} \Delta t k_{off}^R b_R \omega_R \chi_{\Omega_w} + \int_{\Omega} \Delta t k_{off}^R \Delta b_R \omega_R \chi_{\Omega_w} - \int_{\Omega} \Delta t k_{off}^R b_{R0} \omega_R \chi_{\Omega_w} \\
& + \int_{\Omega} b_E \omega_E + \int_{\Omega} \Delta b_E \omega_E - \int_{\Omega} b_E^{old} \omega_E \\
& + \int_{\Omega} \Delta t k_{on}^E c_{all} b_E \omega_E \chi_{\Omega_w} + \int_{\Omega} \Delta t k_{on}^E \Delta c_{all} b_E \omega_E \chi_{\Omega_w} + \int_{\Omega} \Delta t k_{on}^E c_{all} \Delta b_E \omega_E \chi_{\Omega_w} \\
& + \int_{\Omega} \Delta t k_{off}^E b_E \omega_E \chi_{\Omega_w} + \int_{\Omega} \Delta t k_{off}^E \Delta b_E \omega_E \chi_{\Omega_w} - \int_{\Omega} \Delta t k_{off}^E b_{E0} \omega_E \chi_{\Omega_w} \\
& + \int_{\Omega} s \omega_s + \int_{\Omega} \Delta s \omega_s - \int_{\Omega} s^{old} \omega_s \\
& + \int_{\Omega} \Delta t K(s^+)^{2/3} \omega_s \chi_{\Omega_c} - \int_{\Omega} \Delta t K(s^+)^{2/3} c_{all} \omega_s \chi_{\Omega_c} - \int_{\Omega} \Delta t K(s^+)^{2/3} \Delta c_{all} \omega_s \chi_{\Omega_c} = 0.
\end{aligned}$$



# Chapter 4

## Numerical simulations

### 4.1 Approximating parameters of the model

We want to approximate parameters of the mathematical model proposed in section 3.5, for Cypher stent used in in vivo study from section 3.4. Cypher stent, used in the study, has radius of 3.5 mm and length of 18 mm, see [11].

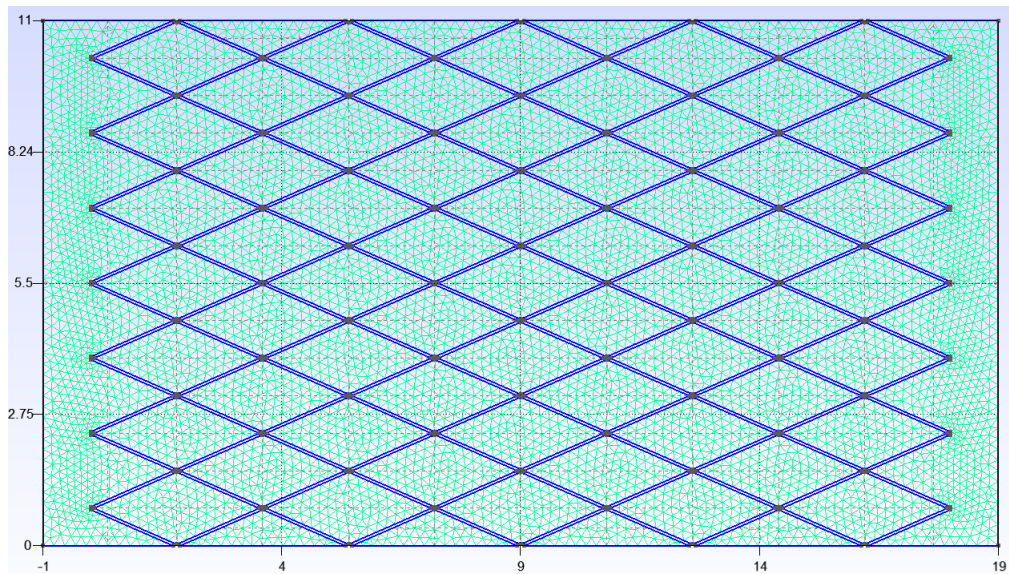


Figure 4.1: Scheme of 2D representation of simplified geometry we use to calculate area and volume of coating. Unit is milimeters (mm).

In Summary of Safety and Effectiveness Data for Cypher Sirolimus-eluting stent, see [22], we see that 3.5 mm diameter stent has seven circumferential cells. Number of cells per length is unfortunately unavailable, so we use the picture of expanded Cypher stent cell and approximate that length/height ratio of one cell of Cypher stent is 4.6/2. To further simplify analysis we assume simple geometry that approximates the geometry of Cyprus stent, consisting of rhombus inscribed in cell that has length of 3.6 mm and height of 1.57 mm. The thickness of stent strut in Cypher stent is approximately 154  $\mu\text{m}$ , where metallic core contributes 140  $\mu\text{m}$ , and polymer layer contributes 14  $\mu\text{m}$  i.e. 7  $\mu\text{m}$  from each side, see [23].

Next, we approximate the volume of the polymer coating and the surface area of the interface. From the schematic representation we can conclude that single cell of stent consists of 4 stent struts of approx. length of 1.96 mm. Stent consists of 35 cells, and cumulative length of stent struts is 274.92 mm. We will estimate volume and surface of stent coating by representing stent as a single stent strut of length 274.92 mm, and idealize cross section of strut as a circle.

$$\text{volume of coating} \rightarrow V \approx 274.92 \times (0.077^2\pi - 0.07^2\pi) \text{ mm}^3 \approx 0.89 \text{ mm}^3$$

$$\text{interface surface area} \rightarrow A \approx 274.92 \times 0.154\pi \text{ mm}^2 \approx 133.01 \text{ mm}^2$$

As we can see, volume of coating is extremely small in comparison with surface area of coating interface. Higuchi's equation in conjunction with data from experiment [19] can be used to approximate diffusivity coefficient in the coating,  $D_c$ . Two crucial assumptions under which Higuchi derived his equation are that the drug is finely dispersed and homogeneously distributed throughout the coating. In case of the Cypher eluting stents, imaging studies showed accumulation of drug dispersed in coating near the interface and consequently significantly elevated concentrations of dispersed drug near the interface, see [11]. We take this information into consideration and perform linear regression on data from [19].

Linear regression is performed for predictor variable, square root of time, and response variable, cumulative amount of drug eluted up until that time. We assume an initial loading of 175  $\mu\text{g}$  as in [11]. Regression line fits the data well, but we can notice that it predicts that 58.2  $\mu\text{g}$  of drug is eluted immediately, see figure 4.2. We will treat this initial immediate jump of amount of eluted drug as a manifestation of anomalous distribution of drug in the coating. Drug is finely dispersed and homogeneously distributed throughout the coating, except near the interface, where it has a sudden and significant jump in concentration. We assume excess of drug is rapidly eluted, high flow-through rate renders the concentration of

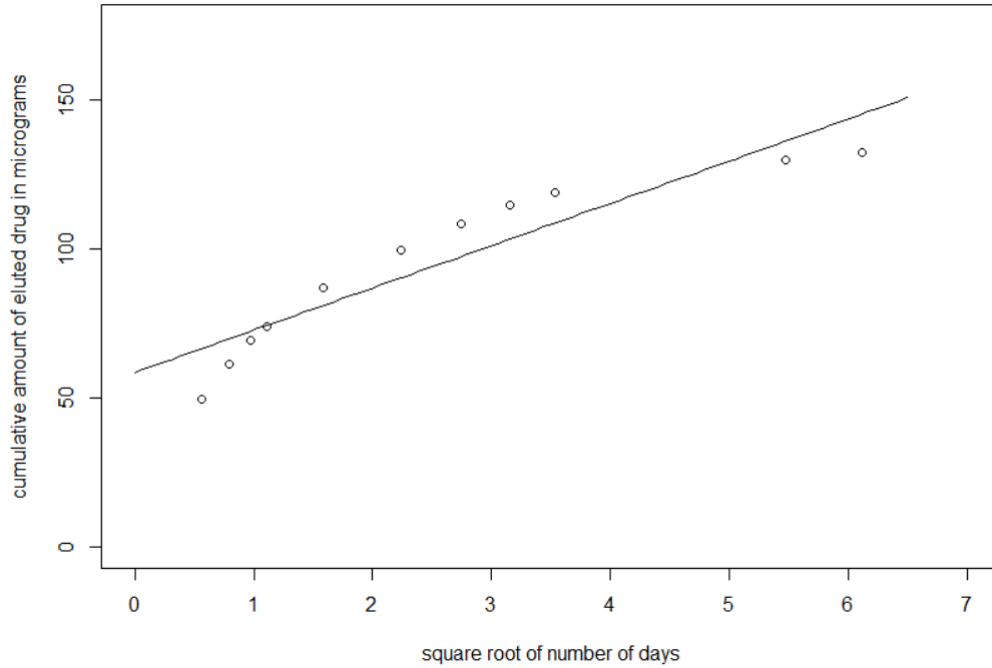


Figure 4.2: Linear regression performed on data from [19] using R. Slope of the regression line is 14.18 and intercept is located at 58.2. P-value is significant, of order  $10^{-5}$ , for both the slope and the intercept.

drug in bulk solution null, and concentration of drug through the coating becomes uniform. From that time point, up until there is no remaining solid drug in the coating, assumptions required for use of Higuchi's equation apply. We note that authors of [11] utilized similar assumptions and derived Higuchi's constant of  $13.22 \mu\text{g}/\sqrt{d}$ .

Under our assumptions there is  $58.2 \mu\text{g}$  of excess drug distributed near the interface and the rest of the drug,  $116.8 \mu\text{g}$ , is uniformly distributed through the coating with concentration of  $131.24 \mu\text{g}/\text{mm}^3$ . Equating slope of the regression line from figure 2 and Higuchi's constant we obtain

$$14.18 (\mu\text{g}/\sqrt{d}) = 133.01 (\text{mm}^2) \sqrt{[2 \times 131.24 - 0.00238] 0.00238 (\mu\text{g}^2/\text{mm}^6) D_c (\text{mm}^2/d)}.$$

Therefore

$$D_c \approx 0.01795 \text{ mm}^2/\text{d}.$$

We used calculated concentration of drug in the coating, and maximum solubility of sirolimus

in water proposed in [24].

Diffusivity of drug in arterial wall  $D_a$ , concentration of drug binding sites  $b_{R0}$ ,  $b_{E0}$  and association/dissociation constants  $k_{on}^E$ ,  $k_{on}^R$ ,  $k_{off}^E$ ,  $k_{off}^R$  are taken from [11] and shown in the table below. Since our model uses dimensionless concentrations, we adapt the parameters by fixing  $c_s = 2.6 \mu\text{M} = 0.00238 \mu\text{g}/\text{mm}^3$ .

Parameter	molar concentrations, mixed units	dimensionless concentrations
$D_c$	0.01795 mm <sup>2</sup> /d	$7.48 \cdot 10^{-4}$ mm <sup>2</sup> /h
$D_a$	$2.00 \times 10^{-6}$ cm <sup>2</sup> /s	0.72 mm <sup>2</sup> /h
$k_{on}^E$	$0.002 \mu\text{M}^{-1}\text{s}^{-1}$	18.72 h <sup>-1</sup>
$k_{on}^R$	$0.8 \mu\text{M}^{-1}\text{s}^{-1}$	7488 h <sup>-1</sup>
$k_{off}^E$	$5.2 \times 10^{-3} \text{s}^{-1}$	18.72 h <sup>-1</sup>
$k_{off}^R$	$1.6 \times 10^{-4} \text{s}^{-1}$	0.576 h <sup>-1</sup>
$b_{E0}$	363 $\mu\text{M}$	139.62
$b_{R0}$	3 $\mu\text{M}$	1.15
$s_0$	131.24 $\mu\text{g}/\text{mm}^3$	55142.86

To approximate dissolution constant  $K$ , we make the assumption that drug is dispersed in the coating in form of spherical particles, as discussed in section 3.1. We set the initial radius of solid sirolimus particle to  $r = 750$  nm. We will first calculate  $N$ ,  $d$  and  $v(0)$ , number of particles in the coating, density of drug in the particle and initial volume of particles. Let  $v_p$  be initial volume of single particle. Let  $v_c$  be volume of cube that contains the particle. Let  $w(0)$  be initial amount of solid drug in the coating.

$$N = \frac{V}{V_c} \approx 217285156,$$

$$v(0) = \frac{V_p}{V_c} V \approx 0.466 \text{ mm}^3,$$

$$d = \frac{w(0)}{v(0)} \approx 250.64 \mu\text{g}/\text{mm}^3.$$

Dissolution constant  $K$  is given by

$$K = \frac{D_c}{h} 4N\pi \left( \frac{4}{3}N\pi \right)^{-2/3} d^{-2/3} V^{-1/3} c_s^{2/3}.$$

Only thing left to define is  $h$ , thickness of the diffusion layer. We will set  $h = 154 \mu\text{m}$ , equal to the thickness of stent strut. We set  $h$  like this because we will set the coating domain through the whole thickness of the stent strut in numerical simulations. We obtain

$$K = 0.00675 \text{ h}^{-1}.$$

Now we have all parameters needed to set up numerical simulations. We notice that density of receptors of type  $R$  makes less than 1% of all receptors sirolimus binds to. The association constant for receptors of type  $R$  is more than 400 times larger than the association constant for receptors of type  $E$ . Association constant for receptors of type  $R$  is 10000 times larger than dissociation constant for the same receptors. Dissociation constant for receptors of type  $R$  is only 4% of value of dissociation constant for receptors of type  $E$ . We can conclude that dynamics associated with receptors of type  $R$  have negligible effect on concentration of drug in the artery because they represent a small fraction of all receptors sirolimus binds to. Receptors of type  $R$  also become saturated rapidly due to high association and low dissociation constants. From that perspective, this type of receptor is not interesting to us because it does not require high concentration of drug to become and stay saturated. Rise in concentration of bound receptors of type  $E$  can serve as an indicator of saturation of receptors of type  $R$ . For these reasons we will neglect receptors of type  $R$  in our numerical simulations.

## 4.2 Results of numerical simulations

We conducted numerical simulations for 3 different stent cell geometries. Simulations required small time step and relatively fine discretization of space domain in the coating and in the vicinity of interface to be stable. Computational time was a major obstacle, so we compromised and utilized a relatively rough mesh, but still fine enough for the simulations to be stable. In programme we used Lagrange P2 elements, i.e. piecewise quadratic finite elements, to approximate  $c_{all}$ . P2 elements are continuous across triangle boundaries, ensuring that  $c_{all}$  is continuous across the interface. For functions  $b_E$  and  $s$  we used P1dc elements, i.e. piecewise linear finite elements. P1dc elements are discontinuous across triangle boundaries. We utilized discontinuous functions because  $b_E$  and  $s$  are relevant only on one part of the domain, and we wanted to ensure that they have no effect on the other part of the domain. Time step was fixed to  $\Delta t = 0.01$  h. Discretization of the space domain is illustrated in figure 4.3.

The biggest constraint we faced was computational time. Obtaining simulations for a span of 7 days, post DES implantation, took approximately 15 h. Sirolimus drug eluting stents elute drug in span of weeks to months. As we will see from results of the simulations, our analysis is restricted to the first phase of drug elution, as described in section 3.2. In this phase, there is no location in the coating that is free of solid drug.

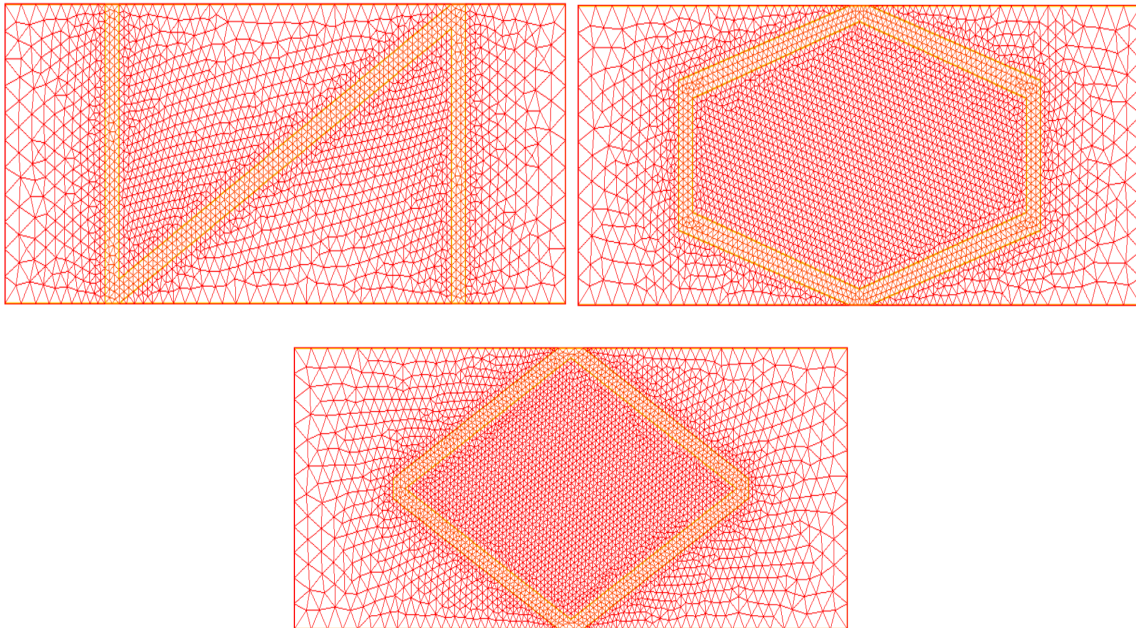


Figure 4.3: Space domain discretization of 3 different stent cell designs.

### Minimum and maximum values of $c_{all}$ on the domain $\Omega_c$

First we focus on the domain  $\Omega_c$ , i.e. the coating. We take a look at behaviour of  $c_{all}$  on this domain. In figure 4.4., up, we see that in the first half hour maximum concentration of  $c_{all}$  in the coating reaches approximately 1, for all 3 cases. Ideally it would reach exactly 1, but due to rough mesh and discontinuous functions that approximate  $s$  in the coating and interact with  $c_{all}$  we have some irregularities. In figure 4.4, down, we can see that maximum value gets closer to 1 as time increases, for all 3 cases. Minimum value of  $c_{all}$  rises as we can see in figure 4.5. Highest value is reached for cell with hexagon shaped, intermediate for Z shaped and lowest for rhombus shaped coating geometry. In the figure 4.6. we see plot of  $c_{all}$  at time  $t = 120$  h, on rhombus shaped coating geometry. Values in the middle are approximately 1. Maximum values, larger than 1, are located near the upper and lower frame line. Similar situation is observed for all 3 geometries.

### Minimum and maximum values of $s$ on the domain $\Omega_c$

Next we take a look at minimum and maximum values of  $s$  in the coating in figure 4.7. We can see that smallest minimum values are reached for cell with rhombus shaped coating geometry, intermediate for Z shaped, and highest for hexagon shaped coating geometries. In the same figure we also see maximum values of  $s$ . Smallest maximum values are reached for cell with rhombus shaped coating geometry, intermediate for Z shaped, and highest for hexagon shaped coating geometry.

We take a closer look at plot of  $s$ . Plot is made in ParaView, open source visualization application. ParaView utilizes P0 elements, i.e. functions that are constant on triangles. In 4.8, on the left we see the plot of  $s$  at time  $t = 120$  h. Mesh has only 3 rows of triangles across the coating thickness. We can see that the highest values are centered in the middle row. Triangles adjacent to the middle row have lower values and triangles adjacent to interface the lowest. In the same figure, on the right, is a histogram of values of  $s$  in the plot. We can see that values of  $s$  averaged on triangles are not higher than the initial value  $s_0$ . We can conclude that values of  $s$  that exceed the initial value are not prevalent, and are likely the consequence of rough mesh combined with P1dc elements used for approximation. Equivalent situation is observed for the other two geometries.

### Minimum and maximum values of $c_{all}$ and $b_E$ on domain $\Omega_w$

In the figure 4.9 we see the plot of minimum values of  $c_{all}$  and maximum values of  $b_E$  on domain  $\Omega_w$ . As we can see, values of minimum concentration  $c_{all}$  are negatively correlated with maximum values of  $b_E$ , concentration of free receptors, as expected. Equivalent situation is observed for maximum values of  $c_{all}$  and minimum values of  $b_E$ , as depicted in figure 4.10.

### Comparisons of cumulative amount of $c_{all}$ , $s$ , $b_E$ for different stent geometries

We want to track how much of the solid drug has dissolved up until time point  $t$ . We calculated initial cumulative concentration of solid drug  $s$  for all 3 cases, and plotted the difference between initial cumulative concentration of solid drug and cumulative concentration of solid drug at time  $t$ , as seen in figure 4.11, on the left. The largest concentration of solid drug that dissolved up until time  $t$  is observed for hexagon shaped, intermediate for Z shaped, and lowest for rhombus shaped coating geometry. In zero sink conditions we would expect to see that cumulative concentration of dissolved drug is positively correlated with area, or in our case length, of the interface and that the same concentration of solid

drug is dissolved per unit length. Hexagon coating geometry has largest length of the interface, Z shaped intermediate, and rhombus shaped the smallest. In that regard cumulative concentration of dissolved solid drug is positively correlated with length of the interface. In the same figure on the right we see that length of the interface is not the only predictor of cumulative concentration of dissolved solid drug since differing cumulative concentrations of dissolved solid drug are observed per unit length of the interface for different geometries. This is expected because we do not have zero sink conditions, concentration of drug in the artery modulates elution of drug from the coating.

Next we observe cumulative concentration of dissolved drug  $c_{all}$  in the artery and cumulative amount of free receptors  $b_E$  in the artery, depicted in figure 4.12. On the left we can see that cell with hexagon shaped geometry has the largest cumulative concentration of  $c_{all}$ , and cells with Z shaped and rhombus shaped coating geometry have similar values, both significantly lower than ones for hexagon shaped coating geometry. Values for rhombus shaped coating geometry are slightly larger than ones for Z shaped coating geometry. On the right we see cumulative concentration of free receptors  $b_E$  is lowest for hexagon shaped coating, as expected since cumulative concentration of dissolved drug is significantly larger for the hexagon shaped coating than for the other two geometries. Cumulative concentration of dissolved drug in the artery is not negatively correlated with cumulative concentration of free receptors, as was the case for minimum/maximum concentration of  $c_{all}$  and maximum/minimum concentration of  $b_E$  in the previous subsection. The reason likely lies in differing geometries modulating distribution of concentration of dissolved drug in the artery wall, as seen in figure 4.14. Concentration of free receptors for differing geometries of the coating can be observed in figure 4.13. As expected locations of highest concentration of dissolved drug in the artery wall coincide with locations of lowest concentration of free receptors. We look at the graph of cumulative concentration of both dissolved free drug in the wall and drug bound to the receptors, in figure 4.12, down. We can see that the largest values are reached for hexagon shaped coating geometry case, intermediate for rhombus shaped case and lowest for Z shaped case. Such result is expected because we already saw that the largest cumulative concentration of the solid drug that dissolved is achieved for hexagon shaped coating geometry, intermediate for Z shaped and lowest for rhombus shaped.

In conclusion, geometry of stent is a major contributor to differences in distribution of concentration of dissolved drug, and consequently distribution of concentration of free receptors in the artery wall. Differing concentrations of drug in the artery wall modulate elution of drug from the interface of the coating, and we observe differing cumulative concentrations of dissolved solid drug in the coating for different DES geometries, indicating that the DES geometry also contributes to differences in duration of drug elution from DES.

### Visualization of numerical results

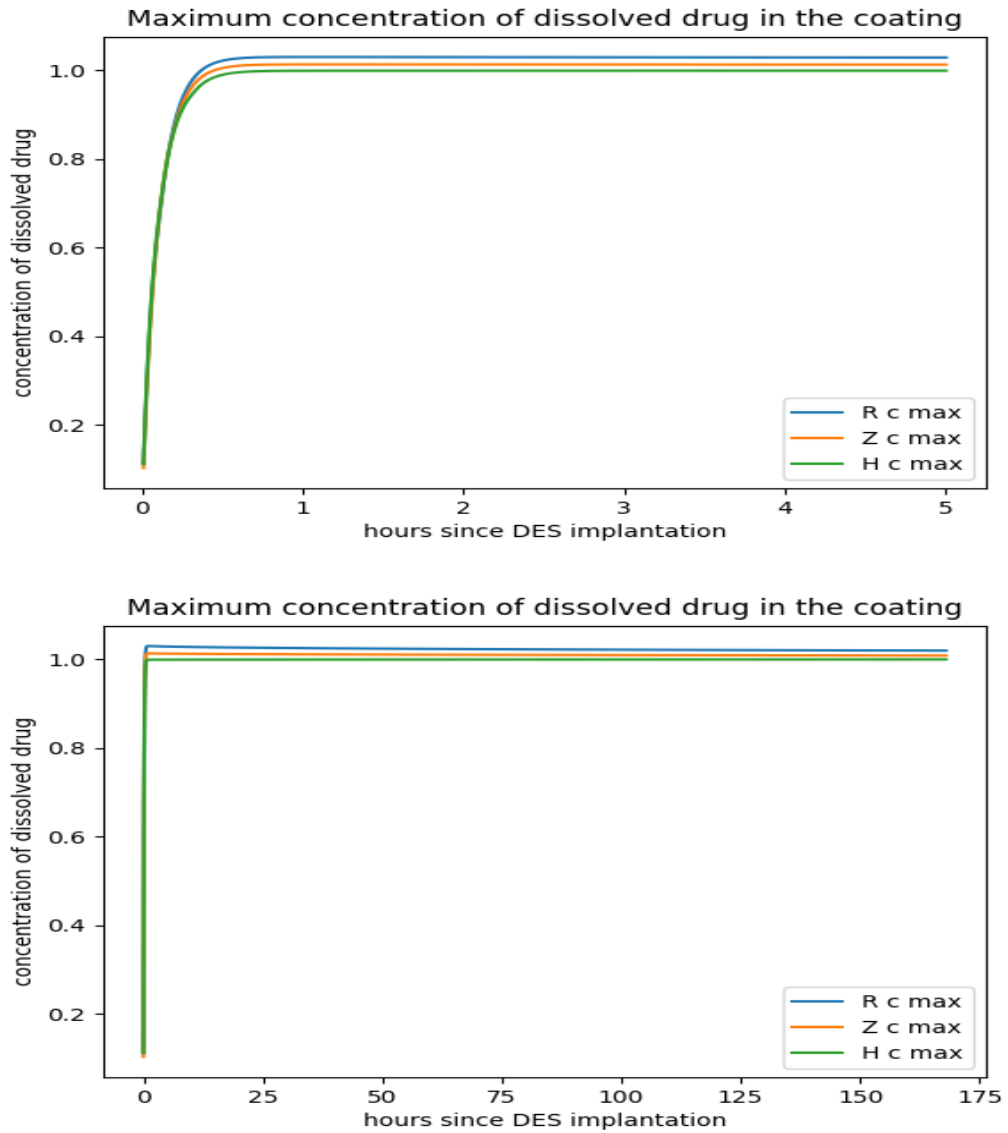


Figure 4.4: Maximum values of  $c_{all}$  in the coating. H represents hexagon shaped, Z Z shaped, and R rhombus shaped geometry.

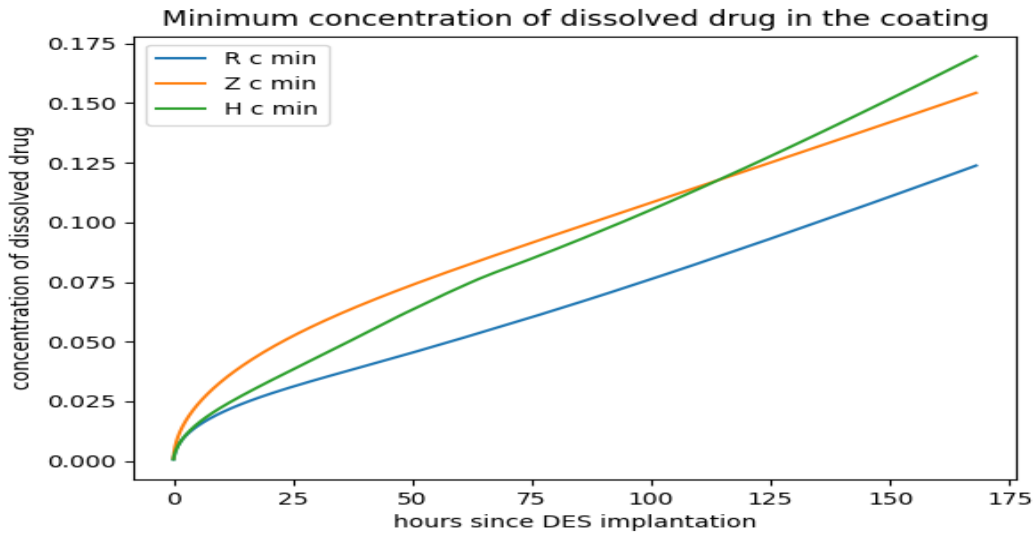


Figure 4.5: Minimum values of  $c_{all}$  in the coating. H represents hexagon shaped, Z Z shaped, and R rhombus shaped geometry.

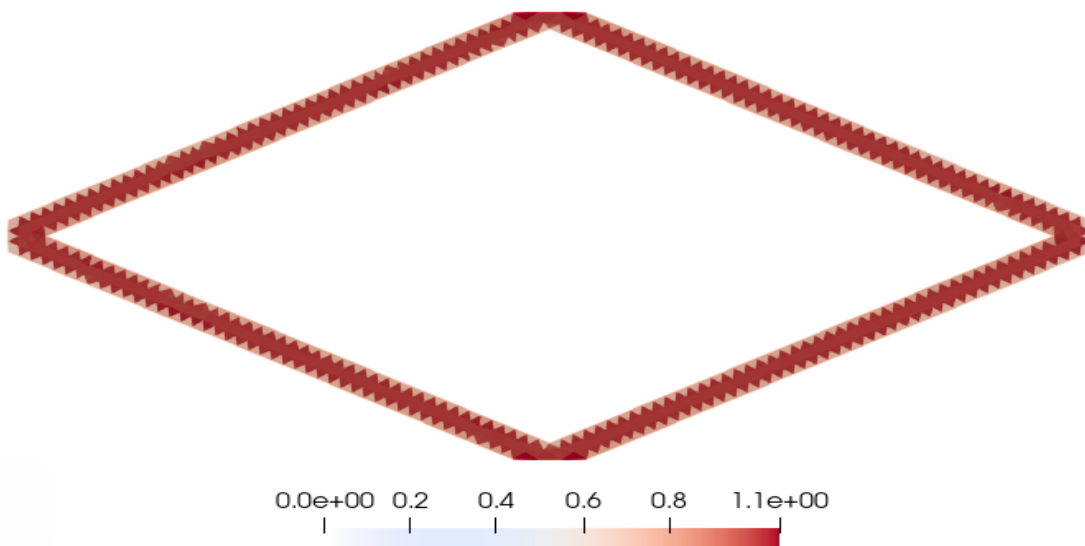


Figure 4.6: Plot of  $c_{all}$  at time  $t = 120$  h, on rhombus shaped coating geometry, obtained in ParaView.

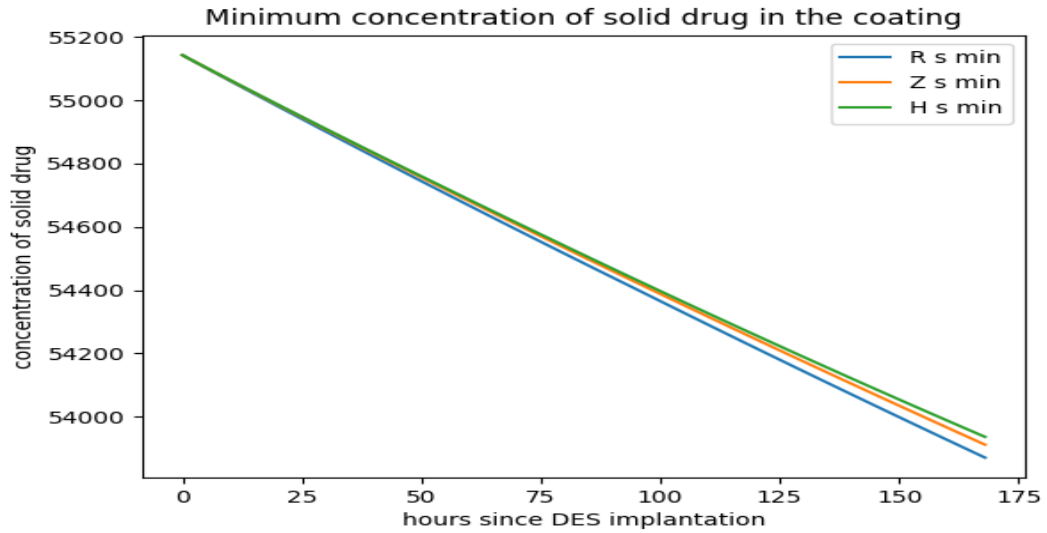


Figure 4.7: Minimum values of  $s$  in the coating. H represents hexagon shaped, Z Z shaped, and R rhombus shaped geometry.

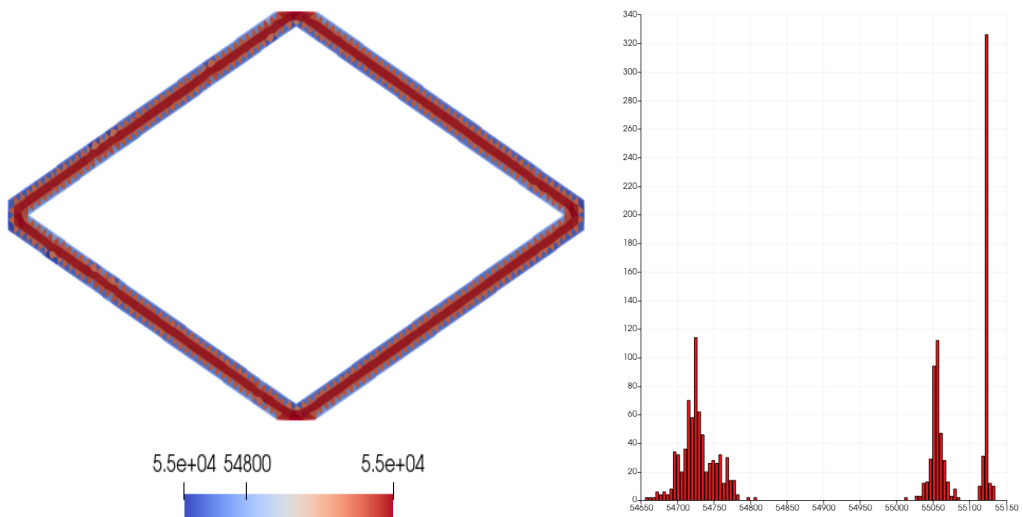


Figure 4.8: On the left, plot of  $s$  at time  $t = 120$  h, on rhombus shaped coating geometry, obtained in ParaView. On the right, histogram of values on the triangles from the plot.

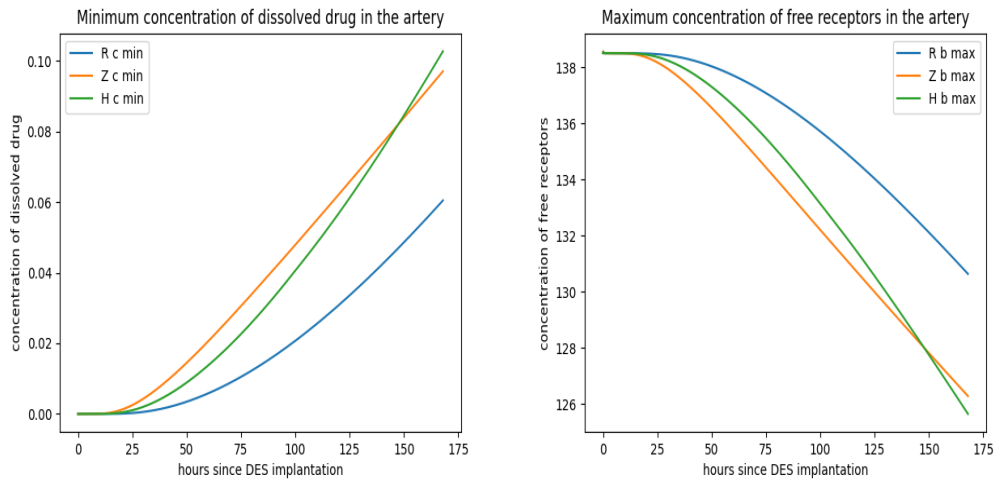


Figure 4.9: Minimum values of  $c_{all}$  and minimum values of  $b_E$  on domain  $\Omega_w$ . H represents hexagon shaped, Z Z shaped, and R rhombus shaped geometry.

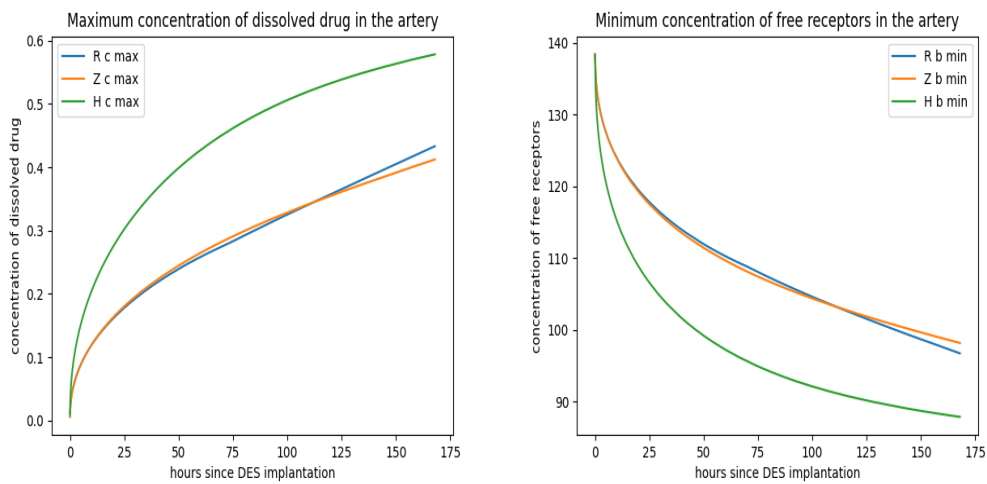


Figure 4.10: Maximum values of  $c_{all}$  and minimum values of  $b_E$  on domain  $\Omega_w$ . H represents hexagon shaped, Z Z shaped, and R rhombus shaped geometry.

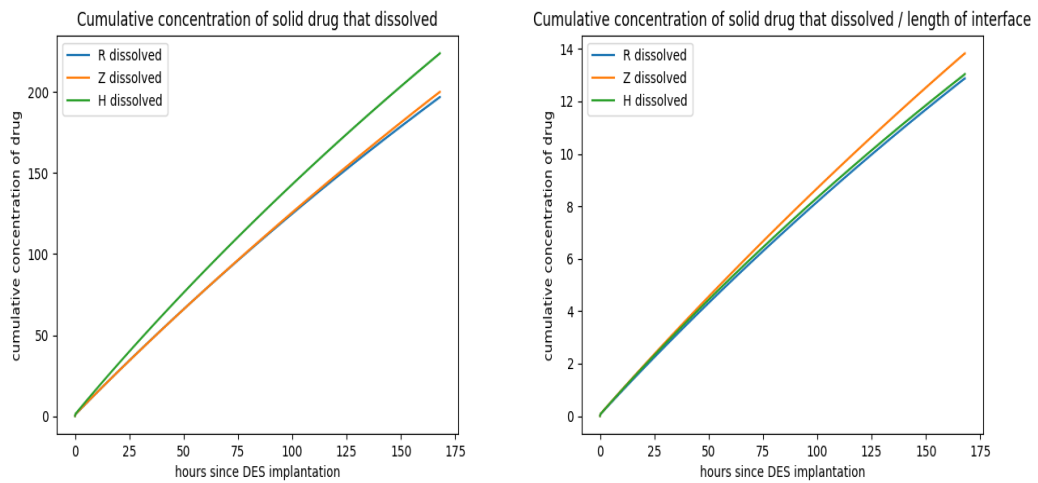


Figure 4.11: On the left, cumulative concentration of solid drug that dissolved up until time  $t$ . On the right, same cumulative concentration divided by length of interface. H represents hexagon shaped, Z Z shaped, and R rhombus shaped geometry.

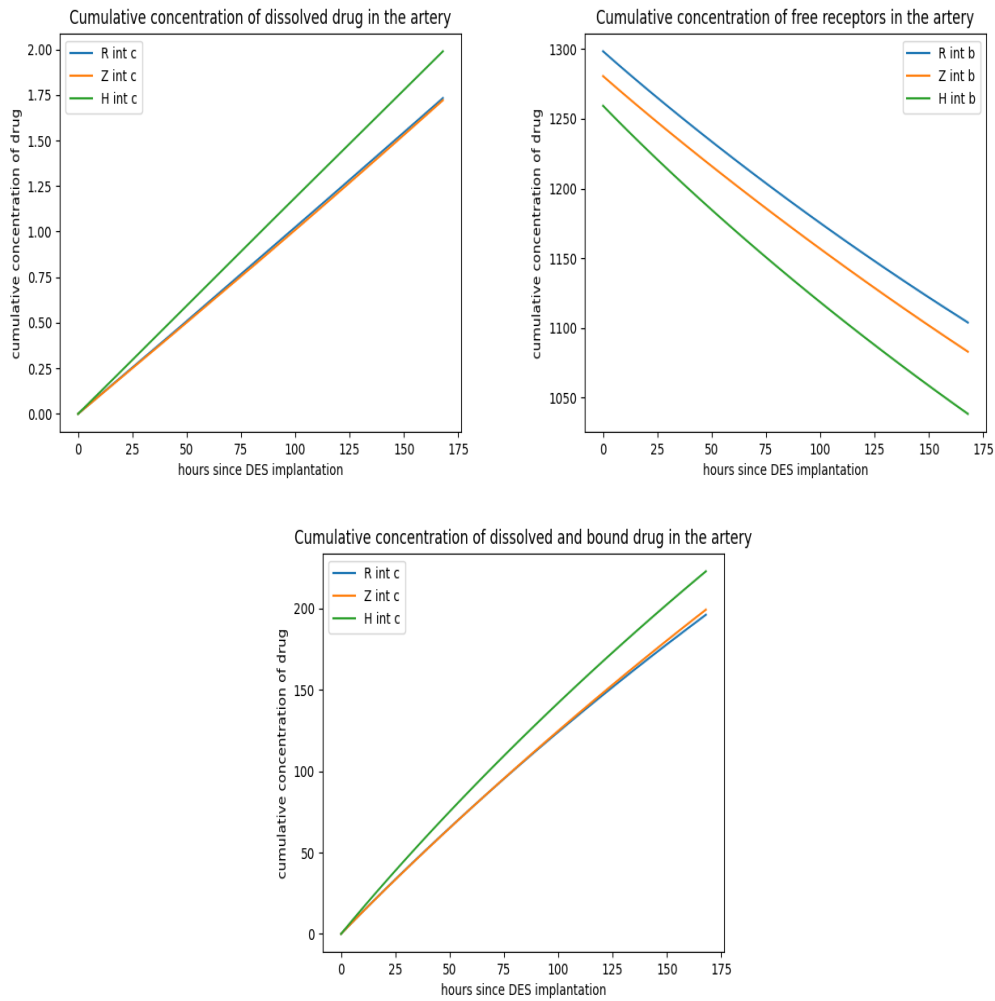


Figure 4.12: Up on the left, cumulative concentration of dissolved drug in the artery. Up on the right, cumulative concentration of free receptors in the artery. Down, cumulative concentration of both free dissolved drug and drug bound to receptors in the artery. and H represents hexagon shaped, Z Z shaped, and R rhombus shaped geometry.

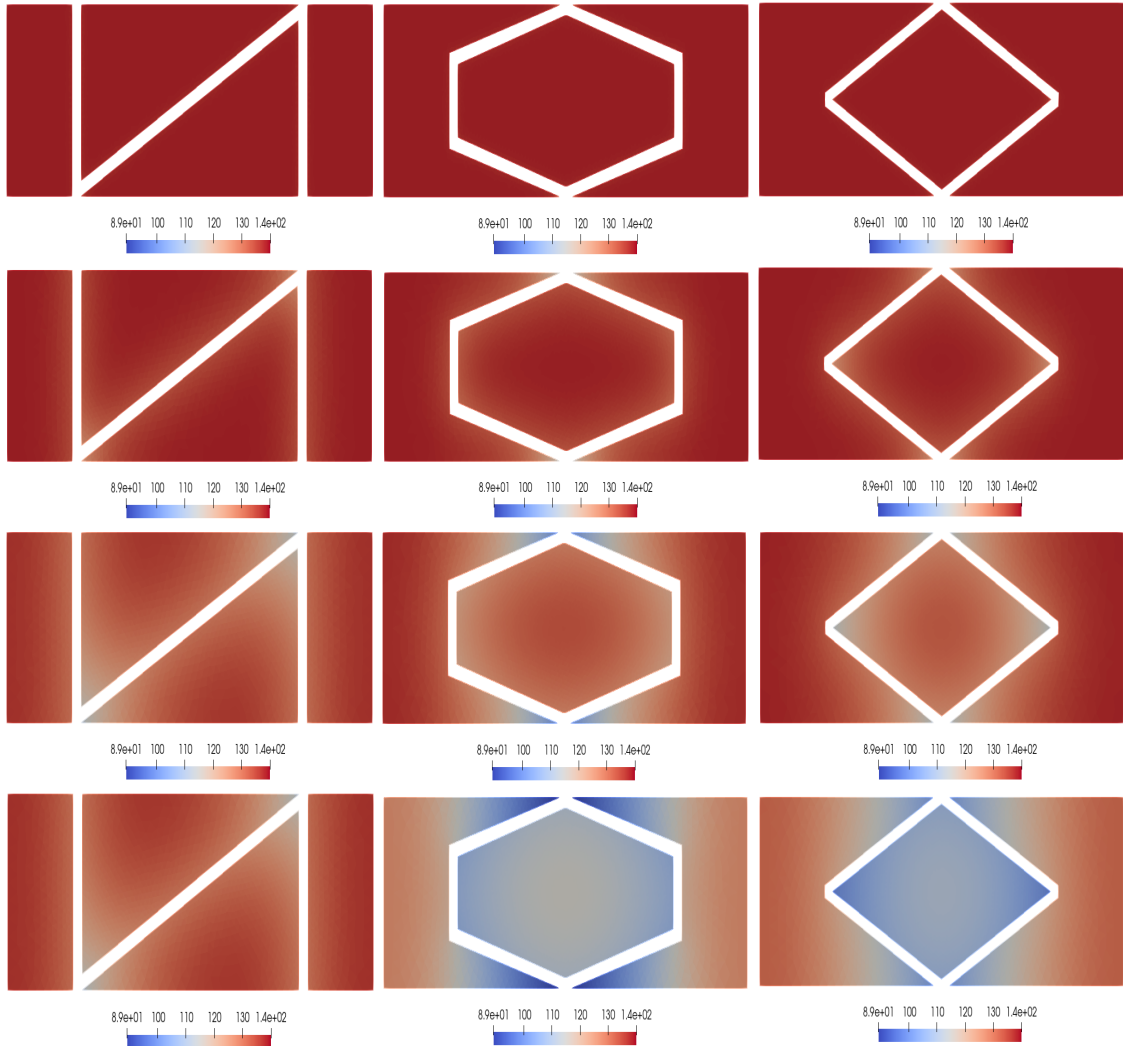


Figure 4.13: Numerical simulation results for  $b_E$ , concentration of free receptors, on the  $\Omega_c$  domain. First row captures  $b_E$  at time  $t = 0.5$  h, second  $t = 12$  h, third  $t = 48$  h and fourth  $t = 160$  h.

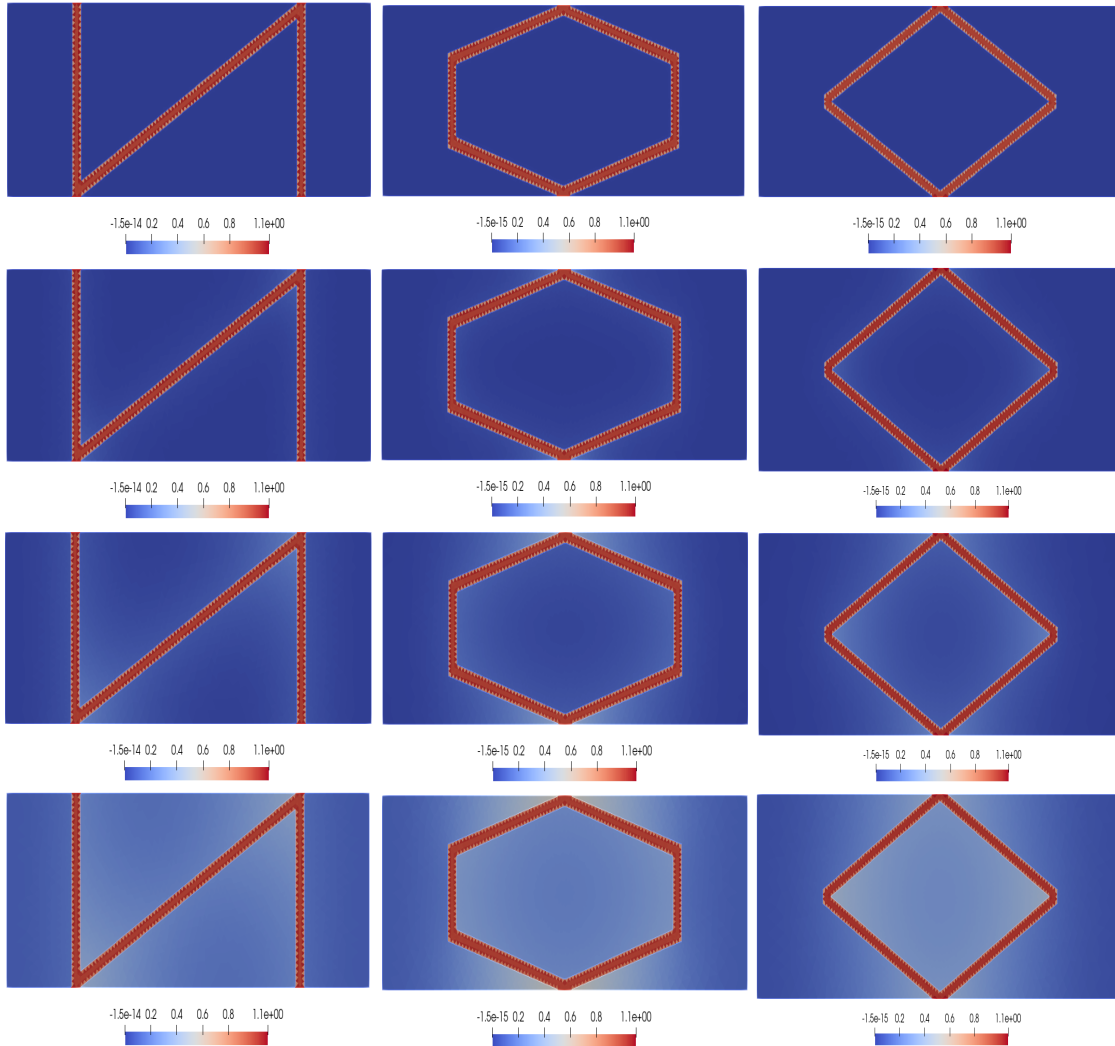


Figure 4.14: Numerical simulation results for  $c_{all}$ , concentration of dissolved drug, on the  $\Omega$  domain. First row captures  $c_{all}$  at time  $t = 0.5$  h, second  $t = 12$  h, third  $t = 48$  h and fourth  $t = 160$  h.

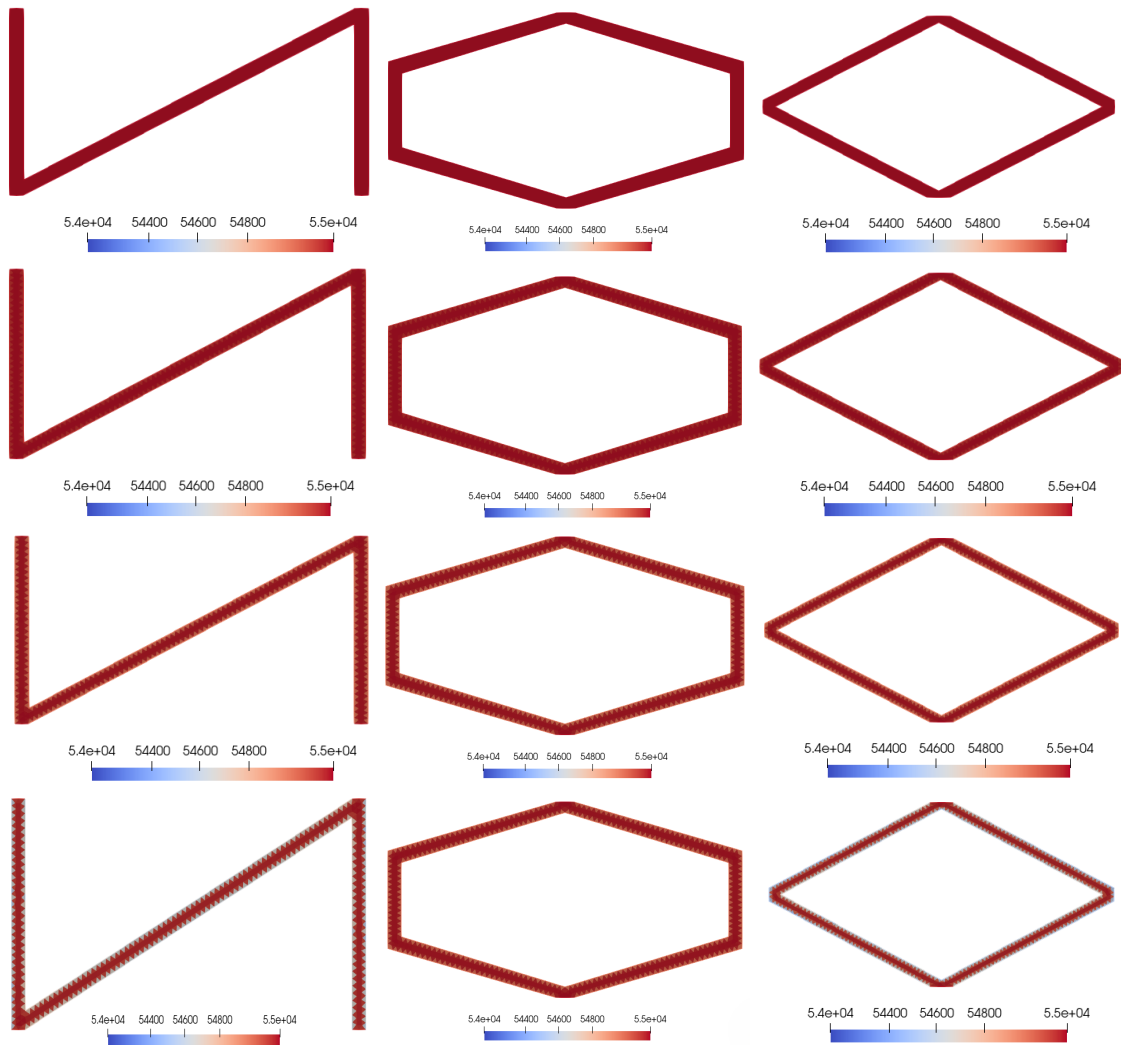


Figure 4.15: Numerical simulation results for  $s$ , concentration of solid drug, on the  $\Omega_c$  domain. First row captures  $s$  at time  $t = 0.5$  h, second  $t = 12$  h, third  $t = 48$  h and fourth  $t = 160$  h.



# Bibliography

- [1] David E. Mohrman and Lois Jane Heller. Cardiovascular physiology, 9th edition. *McGraw-Hill Education*, 2018.
- [2] Shifa Jebari-Benslaiman, Unai Galicia-García, Asier Larrea-Sebal, Javier Rekondo Olaetxea, Iraide Alloza, Koen Vandenbroeck, Asier Benito-Vicente, and César Martín. Pathophysiology of atherosclerosis. *International Journal of Molecular Sciences*, Volume 23, 2022, 3346.
- [3] Peter Libby and Pierre Theroux. Pathophysiology of coronary artery disease. *Circulation*, Volume 111, 2005, 3481-3488.
- [4] Atsushi Shioi and Yuji Ikari. Plaque calcification during atherosclerosis progression and regression. *Journal of Atherosclerosis and Thrombosis*, Volume 25, 2018, 294-303.
- [5] Emil Julian Dabrowski, Marcin Kozuch, and Sławomir Dobrzycki. Left main coronary artery disease—Current management and future perspectives. *Journal of Clinical Medicine*, Volume 11, 2022, 5745.
- [6] Christiaan Vrints, Felicita Andreotti, et al. 2024 ESC guidelines for the diagnosis and management of chronic coronary syndromes: Developed by the task force for the management of chronic coronary syndromes of the European Society of Cardiology (ESC) Endorsed by the European Association for Cardio-Thoracic Surgery (EACTS). *European Heart Journal*, Volume 45, 2024, 3415-3537.
- [7] Juhani Knuuti, William Wijns, et al. 2019 ESC Guidelines for the diagnosis and management of chronic coronary syndromes: The Task Force for the diagnosis and management of chronic coronary syndromes of the European Society of Cardiology (ESC). *European Heart Journal*, Volume 41, 2020, 407-447.
- [8] Robert A Byrne, Xavier Rossello, et al. 2023 ESC Guidelines for the management of acute coronary syndromes: Developed by the task force on the management of acute

- coronary syndromes of the European Society of Cardiology (ESC). *European Heart Journal*, Volume 44, 2023, 3720-3826.
- [9] Sohail Q Khan and Peter F Ludman. Percutaneous coronary intervention. *Elsevier Ltd.*, Volume 50, 2022, 437-444.
- [10] R X Yin, D Z Yang, and J Z Wu. Nanoparticle drug- and gene-eluting stents for the prevention and treatment of coronary restenosis. *Theranostics*, Volume 4, 2014, 175–200.
- [11] A. R. Tzafriri, A. Groothuis, G. S. Price, and E. R. Edelman. Stent elution rate determines drug deposition and receptor-mediated effects. *Journal of Controlled Release*, Volume 161, 2012, 918–926.
- [12] R. Falotico, T. Parker, R. Grishaber, S. Price, and S. A. Cohen. Nevo: a new generation of sirolimus-eluting coronary stent. *EuroIntervention*, Volume 5, 2009, 88-93.
- [13] Avery, Matthew, and et al. Cordis corporation. *Cordis*, 2004.
- [14] Steven Abbott. Solubility science: Principles and practice. *University of Leeds*, 2017.
- [15] D’Angelo, Zunino, Porpora, Morlacchi, and Migliavacca. Model reduction strategies enable computational analysis of controlled drug release from cardiovascular stents. *SIAM Journal on Applied Mathematics*, Volume 71, 2011, 2312-2333.
- [16] G. Frenning. Theoretical investigation of drug release from planar matrix systems: Effects of a finite dissolution rate. *Journal of Controlled Release*, Volume 92, 2003, 331-339.
- [17] Cordis Corporation. A century of dissolution research: From Noyes and Whitney to the biopharmaceutics classification system. *International Journal of Pharmaceutics*, Volume 321, 2006, 1-11.
- [18] A. W. Hixson and J. H. Crowell. Dependence of reaction velocity upon surface and agitation. *Industrial & Engineering Chemistry*, Volume 23, 1931, 923-931.
- [19] Mel Merciadetz, Lori Alquier, R. Mehta, A. J. Patel, and Anchen Wang. A novel method for the elution of sirolimus (rapamycin) in drug-eluting stents. *Dissolution Technologies*, Volume 18, 2011, 37-42.
- [20] Juergen Siepmanna and Nicholas A. Peppasc. Higuchi equation: Derivation, applications, use and misuse. *International Journal of Pharmaceutics*, Volume 418, 2011, 6-12.

- [21] B. Radeleff, H. Thierjung, U. Stampfl, S. Stampfl, R. Lopez-Benitez, C. Sommer, I. Berger, and G. M. Richter. Restenosis of the Cypher-Select, Taxus-Express, and Polyzene-F nanocoated cobalt-chromium stents in the minipig coronary artery model. *Cardiovasc Intervent Radiol.*, Volume 31, 2008, 971-980.
- [22] Summary of safety and effectiveness data. *Cordis*, 2003.
- [23] Jun Tanigawa, Peter Barlis, Konstantinos Dimopoulos, Miles Dalby, and Philip Moore and Carlo Di Mario. The influence of strut thickness and cell design on immediate apposition of drug-eluting stents assessed by optical coherence tomography. *International Journal of Cardiology*, Volume 134, 2009, 180-188.
- [24] M. S. Kim, J. S. Kim, H. J. Park, W.K. Cho, and S.J. Hwang. Enhanced bioavailability of sirolimus via preparation of solid dispersion nanoparticles using a supercritical antisolvent process. *International Journal of Nanomedicine*, Volume 6, 2011, 2997-3009.



# Summary

In this thesis, we develop mathematical model for drug diffusion/dissolution in the coating of drug eluting stent (DES) and drug transport from DES into artery wall. We approximate parameters of the model for sirolimus eluting stent, combining the data for Cypher sirolimus eluting stent from in vivo and in vitro studies. We perform numerical simulations for 3 different drug eluting stent geometries, on a single cell, for a span of 7 days. All 3 cells feature geometries that differ in shape of stent scaffold, but with constant thickness of stent strut, and same initial concentration of same solid drug in the same durable polymer coating. We compare concentrations of dissolved drug and free receptors in the artery wall, and concentrations of solid and dissolved drug in the coating trough time, for different geometries. We conclude that geometry has major effect on distribution of concentration of drug in the artery wall and consequently important effect in distribution of concentration of free/bound receptors in the artery wall. We also notice differences in cumulative amount of solid drug that dissolved and cumulative amount of free and bound drug in the artery wall for different stent geometries. We posit that the effect stent geometry has on distribution of dissolved drug in the artery wall influences elution of drug from DES, resulting in differing elution profiles and length of drug elution from DES.



# **Biography**

I was born on February 10th 1997, in Dubrovnik. I attended Kuna Elementary School in Kuna Pelješka and Gymnasium Dubrovnik, natural sciences and mathematics programme, in high school. I enrolled in the Undergraduate University Study of Mathematics at the Faculty of Science in Zagreb in 2015 and completed my undergraduate studies in 2020. In 2022 I enrolled in the Biomedical Mathematics graduate programme at the same faculty.